Check for updates

ADVANCING EARTH AND SPACE SCIENCES

JGR Earth Surface

RESEARCH ARTICLE
10.1029/2024JF007911

Key Points:

- Mean erosion rates of plateau bedrock are lower than those of cobbles embedded within the Sirius Group
- ^{10}Be and ^{26}Al depth profiles from a 2.95 m permafrost core in the Sirius Group yield an erosion rate of 0.53 m/Myr
- Continual exhumation of embedded clasts from within the Sirius Group results in the formation of an erosional lag deposit

Supporting Information:

Supporting Information may be found in the online version of this article.

Correspondence to:

J. T. H. Anderson,
janderson@ldeo.columbia.edu

Citation:

Anderson, J. T. H., Fink, D., Fujioka, T., Hidy, A. J., Wilson, G. S., Abramov, A., et al. (2025). Constraining erosion rates and landscape evolution with in situ ^{10}Be and ^{26}Al cosmogenic nuclides at Table Mountain, Antarctica. *Journal of Geophysical Research: Earth Surface*, *130*, e2024JF007911. https://doi.org/10.1029/2024JF007911

Received 9 JUL 2024
Accepted 30 JAN 2025

© 2025. The Author(s).
This is an open access article under the terms of the Creative Commons Attribution License, which permits use, distribution and reproduction in any medium, provided the original work is properly cited.

Constraining Erosion Rates and Landscape Evolution With In Situ ^{10}Be and ^{26}Al Cosmogenic Nuclides at Table Mountain, Antarctica

Jacob T. H. Anderson[1,2], David Fink[3], Toshiyuki Fujioka[4], Alan J. Hidy[5], Gary S. Wilson[1,6], Andrey Abramov[7], Nikita Demidov[8], and Klaus Wilcken[3]

[1]Department of Marine Science, University of Otago, Dunedin, New Zealand, [2]Lamont-Doherty Earth Observatory, Columbia University, Palisades, NY, USA, [3]Australian Nuclear Science & Technology Organisation, Lucas Heights, NSW, Australia, [4]Centro Nacional de Investigación Sobre la Evolución Humana, Burgos, Spain, [5]Lawrence Livermore National Laboratory, Center for Accelerator Mass Spectrometry, Livermore, CA, USA, [6]University of Waikato, Hamilton, New Zealand, [7]Institute of Physicochemical and Biological Problems of Soil Science, Pushchino, Russia, [8]Arctic and Antarctic Research Institute, St. Petersburg, Russia

Abstract This study investigates surface weathering and sediment preservation at Table Mountain, a high-elevation, hyperarid, polar landscape in the Transantarctic Mountains. We report cosmogenic nuclide concentrations (^{10}Be and ^{26}Al) in quartz from bedrock surfaces, erratic boulder lag, and cobbles embedded within Sirius Group sediments to quantify erosion rates. In situ ^{10}Be and ^{26}Al depth profiles from a 2.95 m permafrost core in the Sirius Group further constrain surface erosion rates and elucidate landscape stability. Measured ^{10}Be and ^{26}Al concentrations from two sandstone bedrock surfaces adjacent to Sirius Group sediments give erosion rates of 0.18–0.28 m/Myr. An erratic sandstone boulder within the lag above the Sirius Group yields erosion rates of ~0.42 ± 0.03 m/Myr, whereas two cobbles embedded within the Sirius Group yield higher rates of 0.81–1.12 m/Myr. Depth profiles of in situ ^{10}Be and ^{26}Al indicate no vertical mixing of Sirius Group permafrost since deposition. Depth profile models are best explained by erosion rates of $0.53^{+0.13}/_{-0.12}$ m/Myr, and an exposure age of $0.78^{+0.06}/_{-0.08}$ Ma. We view the model "age" to represent the ~0.8-million-year time-scale for surface lowering equivalent to one attenuation length of cosmic ray production to achieve steady-state conditions. Continual exhumation of embedded clasts from within the Sirius Group results in an accumulation of clasts forming the observed erosional lag deposit covering the landscape. Our erosion rates of the Sirius Group surface based on in situ ^{10}Be and ^{26}Al depth profiles are an order-of-magnitude larger than those based on meteoric ^{10}Be infiltration and further clarification is required.

Plain Language Summary High elevation, cold, dry landscapes in the Transantarctic Mountains have some of the lowest erosion rates on Earth. But erosion rates and landscape modification vary on different landscape surfaces. Using geochemical measurements of various geological features such as bedrock surfaces, boulders, glacial sediments, and cobbles embedded within glacial sediments, we calculate erosion rates of these surfaces. Our results show that erosion rates range from 0.18 to 0.28 m per million years in bedrock to up to 1.12 m per million years in embedded cobbles, with higher erosion rates for embedded cobbles and sediments. As embedded cobbles from within the sediments erode, they accumulate on the surface of the glacial sediments, forming a layer of debris. These findings help us understand and compare surface erosion rates from various landforms in one of the coldest and driest regions on Earth.

1. Introduction

Stability of landscapes in the Transantarctic Mountains is being used to infer the longevity of surface strata and rates of Antarctic geomorphic processes (e.g., Sugden et al., 1993, 1995; Valletta et al., 2015; Verret et al., 2023), yet there are conflicting views as to the age of the features being used (e.g., Dickinson et al., 2012; Ng et al., 2005). Antarctic erosion rates are some of the lowest (<0.05–3.5 m/Myr) on Earth (Balter-Kennedy et al., 2020; Marrero et al., 2018). But a compilation of cosmogenic-nuclide derived erosion rate data from across Antarctica shows that the physical setting, elevation, lithology, and sample type (i.e., bedrock, boulder) clearly influence the local rate of erosion (Marrero et al., 2018). Therefore, quantifying erosion rates of these landscapes, and establishing the duration of preservation of glacial sediments since emplacement is critical for understanding landscape evolution, determining the onset of persistent polar climate conditions, and refining past responses of the East Antarctic Ice

10.1029/2024JF007911

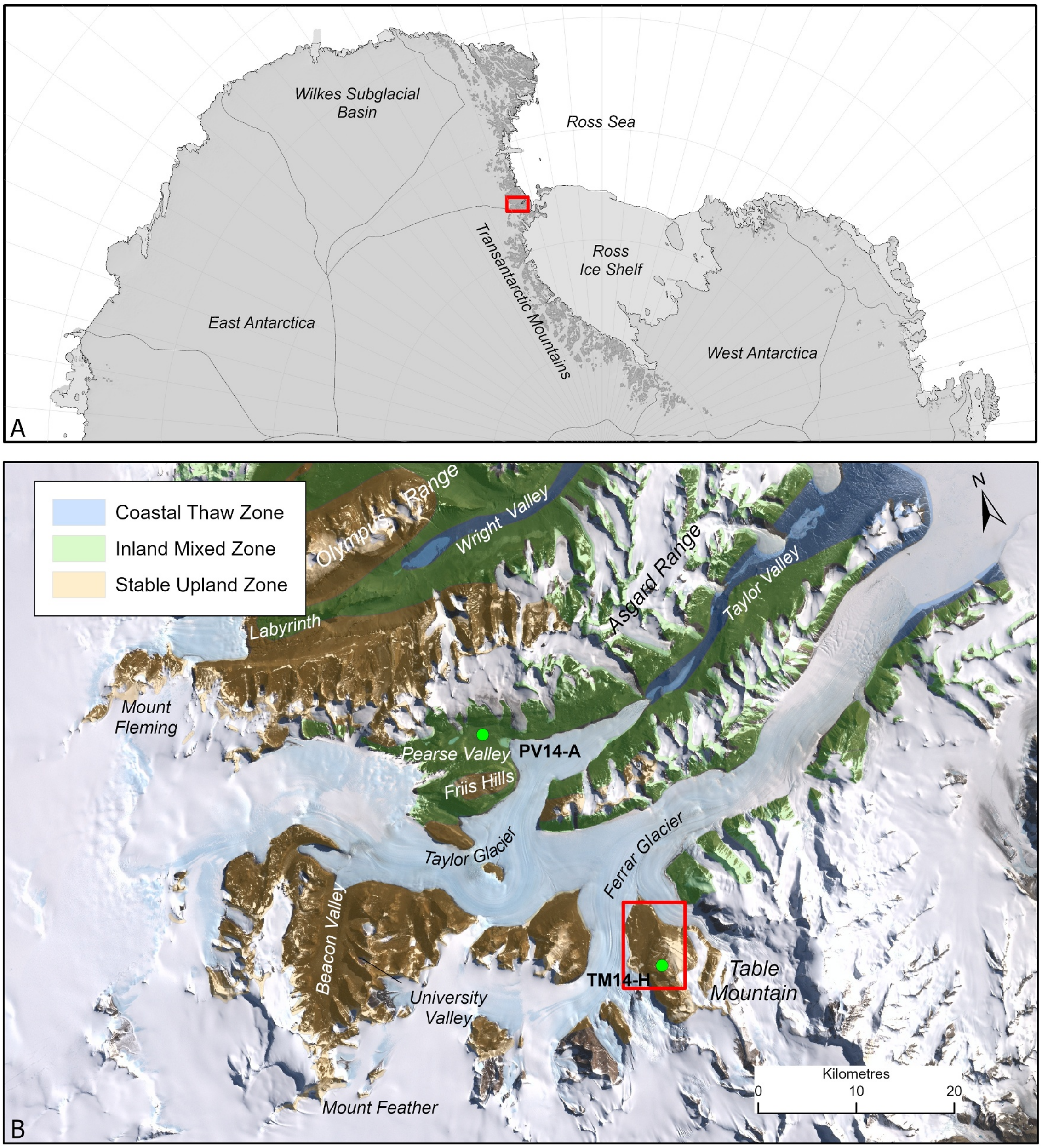

Figure 1. (a) Study area and sites discussed in the text. (b) Location of Table Mountain where the permafrost core (TM14-H) was recovered. Green circles denote core locations, TM14-H, and PV14-A (Anderson et al., 2023). The three microclimatic zones are the stable upland zone (brown), inland mixed zone (green), and coastal thaw zone (blue). Modified from Marchant and Head (2007); and Salvatore and Levy (2021). The red rectangle in the lower diagram shows the location of Figure 2.

Sheet to climate perturbations. The high elevation (>1,000 m) region of the McMurdo Dry Valleys is defined as the stable upland zone (Marchant & Head, 2007), and is classified as a hyperpарid, cold, polar desert climate (Figure 1). A large body of evidence suggests that hyperarid, frozen polar conditions have persisted at high elevation areas in the McMurdo Dry Valleys since the middle Miocene (∼12 Ma) (Lewis et al., 2007; Machant et al., 1993; Marchant & Denton, 1996; Sugden et al., 1993; Valletta et al., 2015). The preservation of Miocene strata, and landforms in the stable upland zone contrasts with evidence showing dynamic marine ice sheet fluctuation during the Pliocene and Pleistocene in the Ross Sea (Fielding et al., 2012; Levy et al., 2012; Naish et al., 2009) and Wilkes Land (Patterson et al., 2014). Despite open marine conditions and reduced marine-based ice sheets in the Ross Sea during past warm intervals, modeling by Halberstadt et al. (2022) suggested that high elevation landscapes in the McMurdo Dry Valleys remained below freezing since the middle Miocene. While ash

21699011, 2025, 3, Downloaded from https://agupubs.onlinelibrary.wiley.com/doi/10.1029/2024JF007911 by University Of Burgos, Wiley Online Library on [12/03/2026]. See the Terms and Conditions (https://onlinelibrary.wiley.com/terms-and-conditions) on Wiley Online Library for rules of use; OA articles are governed by the applicable Creative Commons License

10.1029/2024JF007911

deposits and sediments at many stable upland zone sites are of middle Miocene age (e.g., Chorley et al., 2023; Lewis et al., 2007), several studies from Table Mountain and the Friis Hills argue that the cryostratigraphy and associated minerals in the frozen sediments indicate a persistent polar, arid climate only since the late Miocene (6–9 Ma) (Dickinson et al., 2012; Dickinson & Rosen, 2003; Verret et al., 2023).

Here, we used in situ cosmogenic ^{10}Be and ^{26}Al in quartz from bedrock, an erratic boulder, cobbles embedded within Sirius Group sediments, and in a permafrost core of Sirius Group sediments to assess landscape stability and quantify erosion rates for different sediments at Table Mountain (Figure 1), a high relief region in the stable upland zone. We present companion ^{10}Be and ^{26}Al depth profiles from Sirius Group sediments to determine the surface erosion rate and infer the stability of the landscape surface since deposition. Depth profiles of in situ ^{10}Be and ^{26}Al nuclides in sedimentary deposits in the Transantarctic Mountains have previously been used to determine inheritance of the cosmogenic nuclide inventory, vertical mixing (cryoturbation), surface deflation and quantify erosion rates (Bergelin et al., 2022; Bibby et al., 2016; Morgan et al., 2010, 2011). In the stable upland zone, ^{10}Be and ^{26}Al concentrations from bedrock, boulders and regolith when interpreted as minimum exposure ages are lower than expected (e.g., Ivy-Ochs et al., 1995; Morgan et al., 2010; Putkonen et al., 2008) and are thus best interpreted as steady-state erosion rates of sufficiently long-exposed surfaces (Lal, 1991). Utilizing cosmogenic nuclides, we investigate variations in erosion rates between bedrock, boulders, embedded cobbles, and Sirius Group sediments, and discuss landscape evolution at Table Mountain. Our study provides new insights into post-depositional erosional processes that influence differences between surface denudation of the frozen landscape and the physical weathering of bedrock and erratics during the Pleistocene.

2. Study Site and Geological Setting

Table Mountain is a mountainous ice-free area that flanks the southern side of the Ferrar Glacier and is bounded by the Tedrow Glacier to the west, and the Emmanuel Glacier to the east (Figure 2). Bedrock comprises Cambro-Ordovician Granite Harbor Intrusives, and early Devonian Wind Gully Sandstone, Terra Cotta Siltstone, and New Mountain Sandstone of the Beacon Supergroup Formation, which are intruded by Jurassic sills and dikes of Ferrar Dolerite (Barrett & Powell, 1982). On the north–west side of Table Mountain, glacial and related successions of the Sirius Group overlie Beacon Supergroup and Ferrar Dolerite bedrock, and are at least 9.5 m thick (Figure 2; Goff et al., 2002). The Sirius Group sediments at Table Mountain are subdivided into three facies: gravelly sandstone, sandstone and sandy conglomerate (Barrett & Powell, 1982; Goff et al., 2002). The sediments are predominantly glaciofluvial and glaciolacustrine facies, deposited by wet-based ice from local alpine sources that flowed in a direction similar to that of the present-day Ferrar Glacier (Goff et al., 2002). Dolerite-rich angular pebble and boulder lag drapes much of the Sirius Group deposit and surrounding debris flow at Table Mountain (Barrett & Powell, 1982). The debris flow, an accumulation of supraglacial debris, colluvium and scree, contains Sirius-like sediments, and is assumed to derive largely from the Sirius Group, which has been modified by periglacial processes and mass movement and transported downslope beyond the Ferrar Dolerite sill (Figure 2; Dickinson & Rosen, 2003; Dickinson et al., 2012; Goff et al., 2002). Bedrock and boulders show varying degrees of surface weathering, including weathering rinds, pitting, and cavernous forms (Figure 3).

At Table Mountain, the depositional age of the Sirius Group sediments is inferred to be middle Miocene, based on stratigraphic correlation (Barrett & Powell, 1982; Goff et al., 2002). However, there is no direct age determination of the Sirius Group at Table Mountain and currently it is poorly constrained. Ivy-Ochs et al. (1995) suggested that the Sirius Group has a minimum deposition age of 2.9 Ma inferred by in situ ^{10}Be and ^{26}Al concentrations. Bruno et al. (1997) suggested a probable minimum age of ∼6 Ma using in situ ^{3}He and ^{21}Ne concentrations from boulder samples embedded in, and near the Sirius Group. Post-depositional modifications of Sirius Group sediments at Table Mountain have also been constrained. Dickinson et al. (2012) used a depth profile of meteoric ^{10}Be from illuviated clays within Sirius Group sediments to estimate the onset of hyperarid conditions between 6 and 9 Ma.

Table Mountain has a mean annual surface temperature average between −25 and −30°C (Pringle et al., 2003) and precipitation is <15 mm water equivalent per year (McKay et al., 1998). Ground temperatures in Sirius Group sediments measured in December 1996, decreased from about −5°C at a depth of 0.25 m to −23°C at 3.7 m (Dickinson & Rosen, 2003).

21699011, 2025, 3, Downloaded from https://agupubs.onlinelibrary.wiley.com/doi/10.1029/2024JF007911 by University Of Burgos, Wiley Online Library on [12/03/2026]. See the Terms and Conditions (https://onlinelibrary.wiley.com/terms-and-conditions) on Wiley Online Library for rules of use; OA articles are governed by the applicable Creative Commons License

21699011, 2025, 3, Downloaded from https://agupubs.onlinelibrary.wiley.com/doi/10.1029/2024JF007911 by University Of Burgos, Wiley Online Library on [12/03/2026]. See the Terms and Conditions (https://onlinelibrary.wiley.com/terms-and-conditions) on Wiley Online Library for rules of use; OA articles are governed by the applicable Creative Commons License

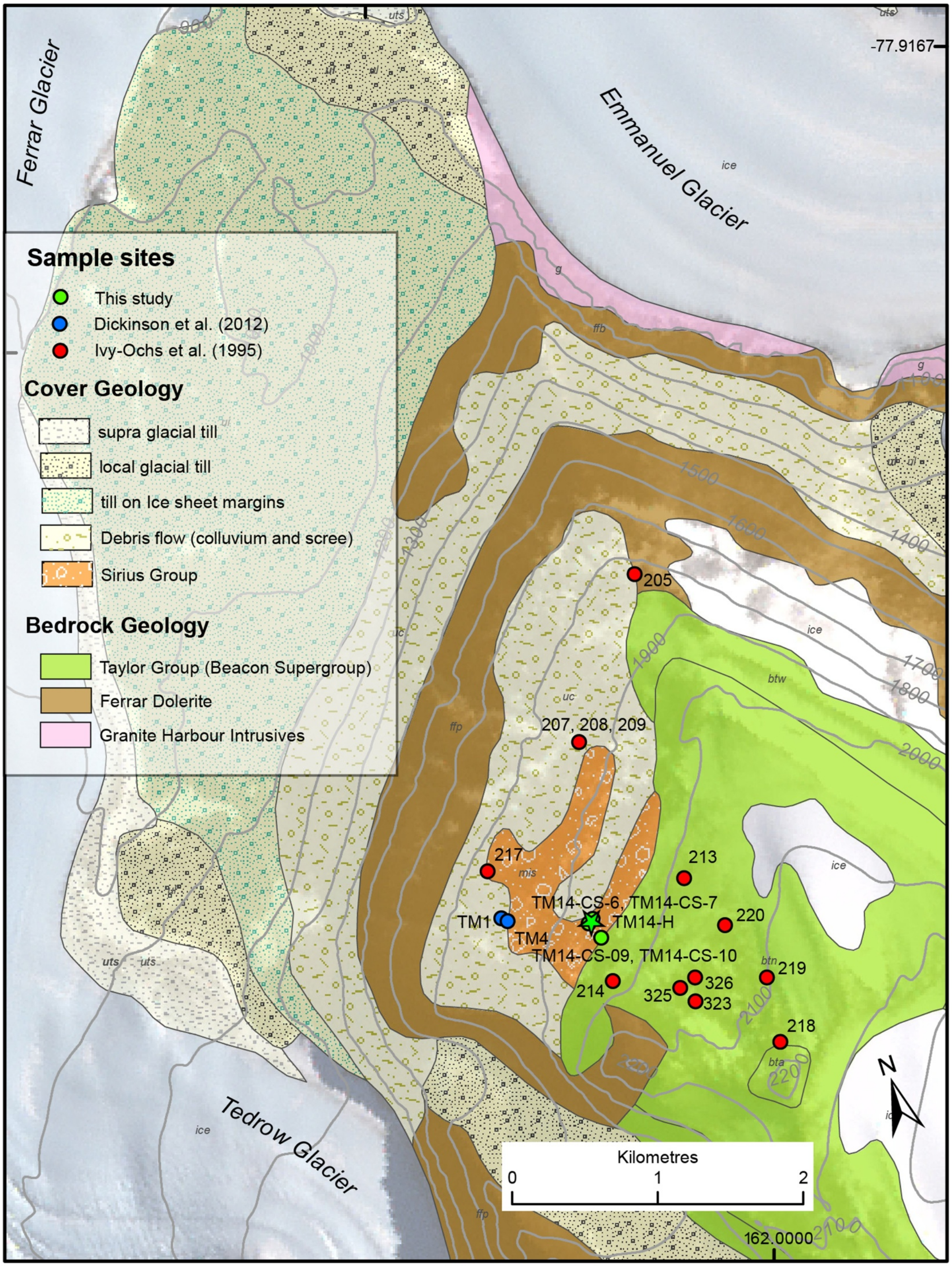

Figure 2. Table Mountain geology and samples from this study (green star denotes core location, TM14-H; green circles denote surface samples), cores TM1 and TM4 (blue circles) from Dickinson et al. (2012), and surface samples (red circles) from Ivy-Ochs et al. (1995). Modified geology from Cox et al. (2012) and references therein. The coordinate data for samples derived from Ivy-Ochs et al. (1995, cf. Panel 2) are inconsistent with the geological map and elevations shown, and locations are approximate.

21699011, 2025, 3, Downloaded from https://agupubs.onlinelibrary.wiley.com/doi/10.1029/2024JF007911 by University Of Burgos, Wiley Online Library on [12/03/2026]. See the Terms and Conditions (https://onlinelibrary.wiley.com/terms-and-conditions) on Wiley Online Library for rules of use; OA articles are governed by the applicable Creative Commons License

Figure 3. (a) Photograph of Beacon sandstone bedrock sample site (TM14-CS09-01, 1,951 m elevation). (b) The bedrock surface displays surface varnish, granular disintegration, and exfoliation weathering. Arrows drawn on the sample indicate the orientation of the upper surface, ensuring accurate interpretation prior to laboratory processing. (c) Photograph of Beacon sandstone bedrock sample (TM14-CS10-01, 1,958 m elevation). The bedrock concretion protrudes above the surrounding bedrock, displaying surface varnish and exfoliation weathering. The brush is 28 cm long. (d, e) Photographs of Beacon sandstone erratic boulder TM14-CS6 at 1,949 m elevation showing the location of samples TM14-CS6-01 and TM14-CS6-02 perched on Sirius Group sediments, ~30 m from the Table Mountain drill site. The boulder and cobble lag of Ferrar Dolerite and Beacon sandstone, which overlies Sirius Group sediments, display pitting and surface varnish. (f) Photograph of Beacon cobble samples (TM14-CS07-01, TM14-CS07-03, TM14-CS07-04) embedded in Sirius Group at 1,945 m elevation near the Table Mountain drill site. Resistant embedded dolerite and sandstone boulders and cobbles lack surface varnish, display no pitting and are shown eroding out of lower density, friable Sirius Group sediments (cf. Figure 2, Goff et al., 2002). Hammer for scale.

3. Methods

3.1. Surface Samples

Seven sandstone surfaces between 1,945 and 1,958 m above present-day sea level were sampled for cosmogenic nuclide analysis (Table 1, Figure 2). Two Beacon sandstone bedrock samples (TM14-CS09-01 and CS10-01), ~100 m south of the drill site, were collected from the nearby Beacon Sandstone plateau surface (Figures 3a, 3b

21699011, 2025, 3, Downloaded from https://agupubs.onlinelibrary.wiley.com/doi/10.1029/2024JF007911 by University Of Burgos, Wiley Online Library on [12/03/2026]. See the Terms and Conditions (https://onlinelibrary.wiley.com/terms-and-conditions) on Wiley Online Library for rules of use; OA articles are governed by the applicable Creative Commons License

and 3c). Two samples were collected from the same Beacon sandstone erratic boulder perched on the Sirius Group (TM14-CS6-01, CS6-02, ∼0.5 m diameter), ∼30 m from the drill site (Figures 3d and 3e). Three Beacon sandstone cobble samples (TM14-CS7-01, CS7-03, CS7-04; all <10 cm diameter), ∼10 m from the drill site, were embedded within surface layers of the Sirius Group deposit (Figures 3f and 4). The coordinates and elevation for each sample were recorded using a handheld GPS receiver, and topographic shielding information was recorded using a compass and inclinometer.

3.2. Permafrost Borehole Core and Characteristics

During the 2014/15 austral field season, permafrost core TM14-H was recovered from Table Mountain using a gasoline powered dry drilling technique (Figures 2 and 5). The core was sampled for sedimentological and cosmogenic nuclide depth profile analysis.

The TM14-H core is located on a ridge of Sirius Group sediments on the north–west side of Table Mountain at 1,948 m above present day sea-level (77.9618°S, 161.98017°E) and was recovered to a depth of 2.95 m (Table 2; Figure 6). Recovered sediments comprise hard, dry permafrost to ∼0.47 m depth, and between 0.47–0.75 m depth contain several clean ice lenses. The quality of core recovery between 0.75–1.09 m depth was poor in many sections, and comprised fractured core and ice-cemented permafrost. Below 1.09 m depth, the recovered sediments were ice-cemented although most of the sandstone sediments had little ice content (2%–10%). Several thin ice lenses were also recovered between 1.47–1.53 m, and 1.88–1.90 m depths. After extraction, the core was divided into ∼10 cm sections for sub-sampling and analysis. Permafrost sediments were collected in a combination of Whirl-Pak bags and PVC core liners. The sediments alternate between fine-medium laminated sandstones, and gravelly sandstone with subangular granules and pebbles of dolerite, granite, quartz arenite and quartz. The recovered core units are associated with the sandstone, and gravelly sandstone facies described by Barrett and Powell (1982) and Goff et al. (2002). We measured 20 ^{10}Be, and 19 ^{26}Al samples for depth profile analysis (Table 2; Figure 6).

3.3. Analytical Methods

Each core sample processed for cosmogenic nuclide analysis was heated at 100°C overnight to remove ice and dry the sediment. Dry core samples, and samples from bedrock, boulder, and cobble surfaces were crushed and sieved to obtain the 250–500 μm fraction. Quartz was separated and purified using the Hot Phosphoric Acid method (Mifsud et al., 2013) and beryllium and aluminum were extracted from quartz via conventional HF dissolution and ion exchange chromatography. Isotope ratios were measured by Accelerator Mass Spectrometry on the 6MV SIRIUS accelerator at the Australian Nuclear Science and Technology Organisation (ANSTO) (Wilcken et al., 2019).

Measured ^{10}Be/^{9}Be ratios were normalized to the 07KNSTD (KN-5.2) standard of Nishiizumi et al. (2007) with a nominal ^{10}Be/^{9}Be ratio of 8.56×10^{-12}. Procedural blanks prepared with a ^{9}Be spike solution derived from deep-mine beryl, used for all the samples in this study, resulted in ^{10}Be/^{9}Be ratios of $1.9 \pm 0.4 \times 10^{-15}$ and $4.8 \pm 1.1 \times 10^{-15}$, and are <2% of the measured ratios for the samples. Measured ^{26}Al/^{27}Al ratios were normalized to the KNSTD (KN-4.2) standard of Nishiizumi (2004) with a nominal ^{26}Al/^{27}Al ratio of 3.096×10^{-11}. Procedural blanks prepared by the ^{27}Al spike solution (ICP Al standard) resulted in ^{26}Al/^{27}Al ratios of $3.5 \pm 1.7 \times 10^{-14}$ and $5.6 \pm 2.8 \times 10^{-14}$, and are <5% of the measured ratios for the samples. All final ^{10}Be/^{9}Be, ^{26}Al/^{27}Al ratios, and quartz and ^{9}Be spike masses are given in Anderson et al. (2025). Tables 1 and 2 display all the nuclide concentration data for the bedrock, boulder, and embedded cobble samples, and depth profiles.

Minimum exposure ages and maximum erosion rates for the erratic, embedded cobbles and bedrock samples were calculated using version 3 of the CRONUS-Earth calculator (http://hess.ess.washington.edu/; Balco et al., 2008) using the LSDn scaling scheme (Lifton et al., 2014) and the primary calibration data set of Borchers et al. (2016). Data for surface samples are archived on the ICE-D Antarctica database (https://www.ice-d.org/antarctica/site/TABLE/).

10.1029/2024JF007911

Table 1
Cosmogenic ^{10}Be and ^{26}Al Concentrations, Apparent Exposure Ages, and Apparent Steady-State Erosion Rates From Table Mountain

Sample name	Latitude (DD)	Longitude (DD)	Elevation (masl)	Sample thickness (cm)[a]	Topographic shielding	^{10}Be conc. (10^7 atoms g^{-1})[b]	^{26}Al conc. (10^7 atoms g^{-1})[c]	Apparent ^{10}Be age (Ma)[d,e]	Apparent ^{26}Al age (Ma)[d,e]	Apparent ^{10}Be erosion rate (m/Myr)[d,e]	Apparent ^{26}Al erosion rate (m/Myr)[d,e]	^{26}Al/^{10}Be ratio
Erratic boulder												
TM14-CS6-01	−77.96180	161.98017	1,949	4	0.999	2.93 ± 0.07	14.16 ± 0.44	1.30 ± 0.12 (0.04)	1.06 ± 0.17 (0.06)	0.37 ± 0.04 (0.02)	0.36 ± 0.09 (0.03)	4.84 ± 0.19
TM14-CS6-02[f]	−77.96180	161.98017	1,949	3	0.999	2.42 ± 0.06	12.14 ± 0.38	0.99 ± 0.08 (0.03)	0.82 ± 0.11 (0.04)	0.52 ± 0.06 (0.02)	0.54 ± 0.11 (0.04)	5.02 ± 0.20
Weighted mean						2.64 ± 0.05	13.00 ± 0.29	1.09 ± 0.07	0.89 ± 0.10	0.42 ± 0.03	0.43 ± 0.07	4.92 ± 0.15
Embedded cobbles												
TM14-CS7-01	−77.96198	161.97855	1,945	2	0.999	1.83 ± 0.04	9.06 ± 0.28	0.70 ± 0.05 (0.02)	0.54 ± 0.06 (0.02)	0.81 ± 0.07 (0.03)	0.95 ± 0.15 (0.05)	4.95 ± 0.19
TM14-CS7-03	−77.96198	161.97855	1,945	4	0.996	1.41 ± 0.03	6.91 ± 0.23	0.53 ± 0.04 (0.01)	0.39 ± 0.04 (0.02)	1.12 ± 0.09 (0.03)	1.42 ± 0.19 (0.07)	4.91 ± 0.20
TM14-CS7-04	−77.96198	161.97855	1,945	5	0.992	0.67 ± 0.02	3.97 ± 0.13	0.24 ± 0.02 (0.01)	0.21 ± 0.02 (0.01)	2.70 ± 0.19 (0.07)	2.93 ± 0.33 (0.11)	5.90 ± 0.23
Bedrock												
TM14-CS09-01	77.9633833	161.97878	1,951	1	0.999	3.42 ± 0.04	17.63 ± 0.68	1.57 ± 0.14 (0.03)	1.57 ± 0.36 (0.15)	0.28 ± 0.04 (0.01)	0.18 ± 0.08 (0.03)	5.15 ± 0.21
TM14-CS10-01	77.9630667	161.98077	1,958	3	0.999	3.53 ± 0.04	17.35 ± 0.67	1.67 ± 0.16 (0.03)	1.55 ± 0.35 (0.14)	0.26 ± 0.04 (0.01)	0.18 ± 0.08 (0.03)	4.92 ± 0.20

Note. All samples are sandstone and have a density of 2.4 g cm^{-3}. [a]Sample thickness was measured in the laboratory using a ruler. [b]Normalized to the 07KNSTD (KN-5.2) standard of Nishiizumi et al. (2007). [c]Normalized to the KNSTD (KN-4.2) standard of Nishiizumi (2004). [d]Exposure ages and erosion rates calculated using the CRONUS-Earth calculator v3 (http://hess.ess.washington.edu/math/), using the LSDn scaling scheme (Lifton et al., 2014) and the primary calibration data set of Borchers et al. (2016). [e]Both internal and external uncertainties (shown at the 1σ level). Internal uncertainties (given in parentheses) are analytical uncertainties only and external uncertainties are absolute uncertainties and include production rate and scaling. [f]duplicate sample taken from top surface of TM14-CS6 and processed in the same batch as CS6-01.

21699011, 2025, 3, Downloaded from https://agupubs.onlinelibrary.wiley.com/doi/10.1029/2024JF007911 by University Of Burgos, Wiley Online Library on [12/03/2026]. See the Terms and Conditions (https://onlinelibrary.wiley.com/terms-and-conditions) on Wiley Online Library for rules of use; OA articles are governed by the applicable Creative Commons License

10.1029/2024JF007911

Figure 4. Photograph of Beacon cobble sample (TM14-CS07-04, 1,945 m elevation) embedded in Sirius Group near Table Mountain drill site. The cobble lacks surface varnish and displays no pitting and is shown eroding out of lower density, friable Sirius Group sediments. TM14-CS07-04 is 7 cm wide.

3.4. Dual Nuclide Depth Profile Models and Parameters

^{10}Be and ^{26}Al data from TM14-H core samples were used to model the surface exposure age and erosion rate of permafrost sediments and inheritance at Table Mountain via the depth profile technique (Anderson et al., 1996). We implemented a modified version of the Monte Carlo-based code of Hidy et al. (2010) that models ^{10}Be and ^{26}Al jointly (after Hidy et al. (2018)). The model iteratively seeks a combination of deposition age, surface erosion rate, and inheritance to best reproduce the measured ^{10}Be and ^{26}Al concentrations for the depth profile within a given percentile (e.g., Hidy et al., 2010, 2018). This modeling approach was successfully applied in a similar study (Anderson et al., 2023) to quantify landscape evolution and permafrost stability using two permafrost cores from Wright Valley and Pearse Valley in the McMurdo Dry Valleys.

21699011, 2025, 3, Downloaded from https://agupubs.onlinelibrary.wiley.com/doi/10.1029/2024JF007911 by University Of Burgos, Wiley Online Library on [12/03/2026]. See the Terms and Conditions (https://onlinelibrary.wiley.com/terms-and-conditions) on Wiley Online Library for rules of use; OA articles are governed by the applicable Creative Commons License

21699011, 2025, 3, Downloaded from https://agupubs.onlinelibrary.wiley.com/doi/10.1029/2024JF007911 by University Of Burgos, Wiley Online Library on [12/03/2026]. See the Terms and Conditions (https://onlinelibrary.wiley.com/terms-and-conditions) on Wiley Online Library for rules of use; OA articles are governed by the applicable Creative Commons License

Figure 5. TM14-H borehole sample site (1,948 m elevation) at Table Mountain.

Table 2
Measured Depth Profile Data From Table Mountain

Sample name	Sample depth (m)	Bulk density (g cm^{-3})	^{10}Be conc. (10^6 atoms g^{-1})[a]	^{26}Al conc. (10^7 atoms g^{-1})[b]	$^{26}Al/^{10}Be$ ratio
TM14-H-01	0–0.07	2.00	15.10 ± 0.21	8.76 ± 0.34	5.81 ± 0.24
TM14-H-02	0.07–0.14	1.80	14.00 ± 0.20	7.82 ± 0.30	5.58 ± 0.23
TM14-H-03	0.14–0.2	1.80	12.56 ± 0.18	7.13 ± 0.28	5.68 ± 0.23
TM14-H-04	0.2–0.3	1.80	11.57 ± 0.18	*3.75 ± 0.15*	*3.24 ± 0.14*
TM14-H-05	0.3–0.42	1.80	10.00 ± 0.15	5.99 ± 0.22	5.98 ± 0.24
TM14-H-06	0.42–0.47	1.40	9.02 ± 0.13	5.08 ± 0.22	5.63 ± 0.25
TM14-H-08	0.55–0.58	1.20	9.66 ± 0.14	5.56 ± 0.26	5.75 ± 0.28
TM14-H-10	0.62–0.72	1.55	7.46 ± 0.10	4.27 ± 0.16	5.72 ± 0.23
TM14-H-13	0.89–0.95	1.70	5.35 ± 0.07	3.08 ± 0.12	5.76 ± 0.24
TM14-H-15	1.01–1.05	1.80	4.31 ± 0.06	2.62 ± 0.10	6.08 ± 0.24
TM14-H-19	1.09–1.19	1.80	3.10 ± 0.05	1.84 ± 0.07	5.93 ± 0.24
TM14-H-20	1.19–1.29	1.60	2.92 ± 0.05	1.63 ± 0.06	5.56 ± 0.23
TM14-H-23	1.47–1.53	1.60	2.15 ± 0.03	1.14 ± 0.06	5.31 ± 0.30
TM14-H-25	1.54–1.62	1.70	2.01 ± 0.03	1.18 ± 0.06	5.84 ± 0.32
TM14-H-26	1.62–1.71	1.60	1.79 ± 0.03	1.01 ± 0.07	5.63 ± 0.43
TM14-H-30	1.99–2.09	1.60	1.13 ± 0.02	0.65 ± 0.04	5.74 ± 0.40
TM14-H-32	2.14–2.24	1.40	0.91 ± 0.02	0.57 ± 0.02	6.25 ± 0.29
TM14-H-35	2.47–2.56	2.05	0.63 ± 0.01	0.36 ± 0.02	5.76 ± 0.33
TM14-H-37	2.64–2.71	1.60	0.50 ± 0.01	0.33 ± 0.03	6.58 ± 0.56
TM14-H-40	2.87–2.95	1.50	0.39 ± 0.01	0.23 ± 0.01	6.03 ± 0.31

Note. Topographic shielding is 0.9993 for TM14-H core. The ^{26}Al concentration for TM14-H-04 (italics) is considered an outlier and not used in the depth profile model. [a]Normalized to the 07KNSTD (KN-5.2) standard of Nishiizumi et al. (2007). [b]Normalized to the KNSTD (KN-4.2) standard of Nishiizumi (2004).

10.1029/2024JF007911

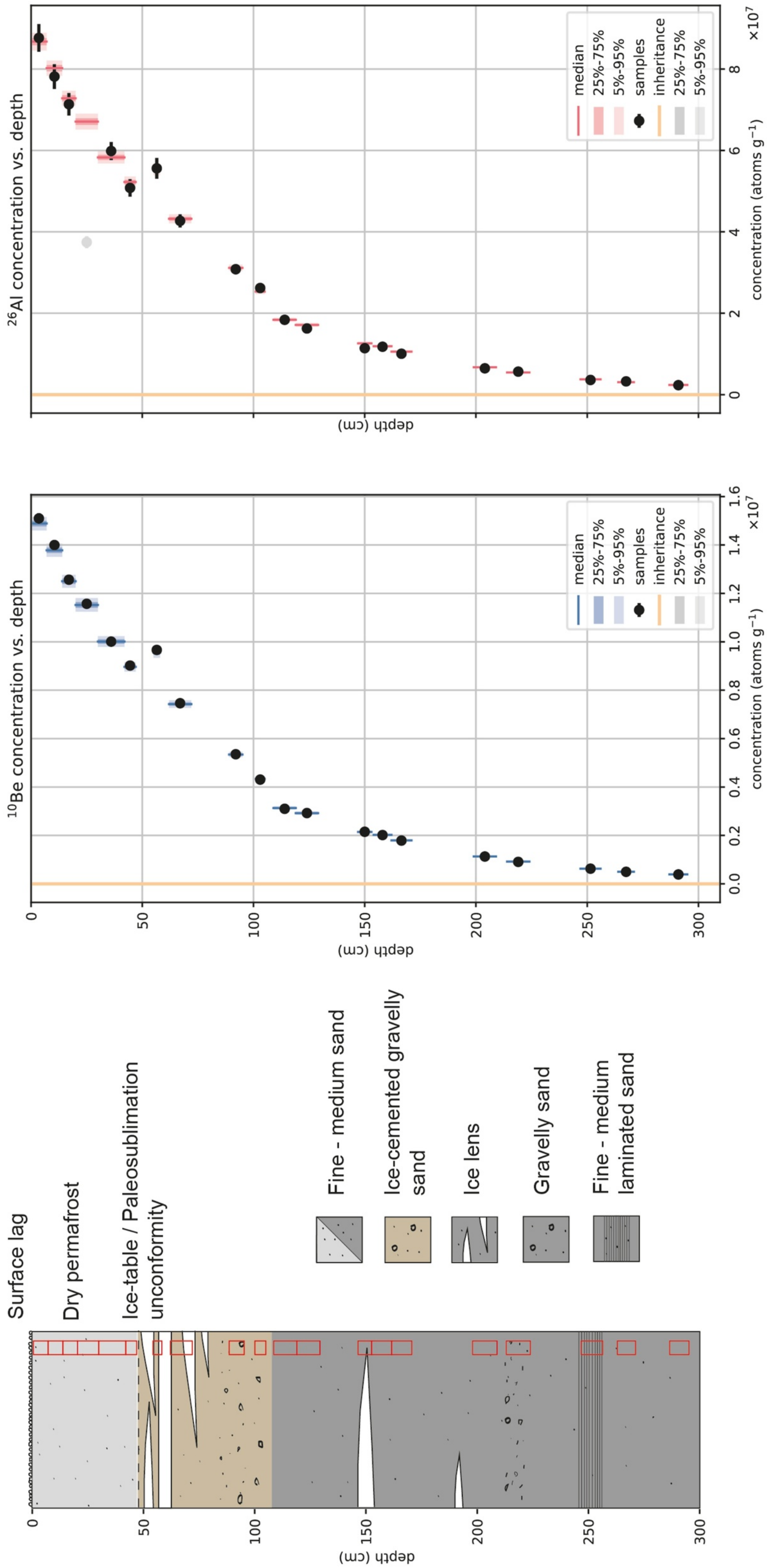

Figure 6. Table Mountain (TM14-H) permafrost core sedimentology (left). Locations of cosmogenic nuclide samples are shown in red boxes. TM14-H permafrost core depth profiles with measured ^{10}Be and ^{26}Al concentrations (black data points) with 1σ uncertainties (right). Measured (gray) ^{26}Al concentration (TM14-H-04) is an outlier, and the sample was excluded from the simulation. Blue (^{10}Be) and red (^{26}Al) boxes show best-fit modeled nuclide concentrations at each sample depth, with their 25th to 75th and 5th to 95th percentiles.

21699011, 2025, 3, Downloaded from https://agupubs.onlinelibrary.wiley.com/doi/10.1029/2024JF007911 by University Of Burgos, Wiley Online Library on [12/03/2026]. See the Terms and Conditions (https://onlinelibrary.wiley.com/terms-and-conditions) on Wiley Online Library for rules of use; OA articles are governed by the applicable Creative Commons License

21699011, 2025, 3, Downloaded from https://agupubs.onlinelibrary.wiley.com/doi/10.1029/2024JF007911 by University Of Burgos, Wiley Online Library on [12/03/2026]. See the Terms and Conditions (https://onlinelibrary.wiley.com/terms-and-conditions) on Wiley Online Library for rules of use; OA articles are governed by the applicable Creative Commons License

To ensure consistency with the exposure ages calculated for the surface samples (Table 1), we assigned the production rates obtained from the CRONUS-Earth calculator to the depth-profile modeling. For the TM14-H core, we used a site-specific spallation ^{10}Be surface production rate of 30.2 atoms ^{10}Be g^{-1} (quartz) yr^{-1}, and a ^{26}Al surface production rate of 211.7 atoms ^{26}Al g^{-1} (quartz) yr^{-1}, which results in a ^{26}Al/^{10}Be surface production rate ratio of 7.00. These production rates were calculated using LSDn scaling (Lifton et al., 2014) and the primary calibration data set of Borchers et al. (2016). We assumed an attenuation length of 140 ± 5 g cm^{-2} for the spallation reaction at depth, as used in previous Antarctic studies (Bergelin et al., 2022; Borchers et al., 2016). Spallogenic production rate uncertainty was not included in the modeling. Muogenic production at depth, including an assumed 8% uncertainty, followed Model 1A from Balco (2017). Bulk density of frozen core samples was measured using the glass bead method (Sheldrick, 1984). Bulk density measurements for the depth profile were between 1.4–2.05 g cm^{-3}, except for the ice lenses, for which we assumed a density of 1.2 g cm^{-3} (Table 2). Within these constraints, deposition age, surface erosion rate, and inheritance for ^{10}Be and ^{26}Al were simulated with uniform distributions in order to reproduce measured ^{10}Be and ^{26}Al concentration profiles within a 5th to 95th percentile error range from a population of 100,000 acceptable paired nuclide depth profile solutions.

4. Results

4.1. Surface Samples at Table Mountain

4.1.1. Bedrock

^{10}Be and ^{26}Al measurements for bedrock samples at Table Mountain are shown in Table 1. Our measured ^{10}Be and ^{26}Al concentrations from two bedrock surfaces (TM14-CS09-01 and TM14-CS10-01) exhibit the highest ^{10}Be concentrations of 3.42 and 3.53 × 10^{7} atoms g^{-1} and give apparent minimum exposure ages between 1.57 and 1.67 Ma. Apparent steady-state erosion rates derived from these ^{10}Be and ^{26}Al bedrock surface concentrations are between 0.18 and 0.28 m/Myr.

Beacon sandstone bedrock from the plateau surface at Table Mountain displays surface varnish, granular disintegration, and exfoliation weathering (Figures 3a, 3b and 3c). Sample TM14-CS10-01 is from a bedrock concretion that protrudes ~30 cm above the surrounding parent bedrock (Figure 3c). The concretion is still part of the bedrock, illustrating that the weathering of the surrounding bedrock is faster than the concretion. This feature is direct evidence that at least ~30 cm of the original plateau surface has been eroded. When plotted on the ^{10}Be–^{26}Al/^{10}Be diagram, both bedrock samples lie within the steady-state erosion island and therefore indicate they have experienced simple exposure histories for at least the last several million years (Figure 7a).

4.1.2. Boulders and Embedded Cobbles

Our ^{10}Be and ^{26}Al measurements for boulders and embedded cobble samples at Table Mountain are shown in Table 1. Two separate samples were taken, about 30 cm apart, from the flat exposed surface of perched Beacon sandstone erratic boulder TM14-CS6 (CS6-01 and CS6-02; see Table 1), with sample CS6-02 giving ^{10}Be and ^{26}Al concentrations, respectively, 17% and 14% lower than for CS6-01 that do not overlap at the 2-sigma uncertainty level. The difference cannot be associated with any analytical error and we surmise that surface modification and/or differences in exposure (i.e., weathering variability) are the causes. For the following discussion, we use the weighted mean and standard mean error of concentrations from samples CS6-01 and CS6-02. This results in apparent ^{10}Be and ^{26}Al minimum exposure ages of 1.09 ± 0.07 and 0.89 ± 0.10 Ma and apparent steady-state erosion rates of 0.42 ± 0.03 and 0.43 ± 0.07 m/Myr, respectively. The three cobbles (TM14-CS7-01, −03, −04) embedded in the Sirius Group returned ^{10}Be concentrations of 0.67–1.83 × 10^{7} atoms g^{-1}, which are much lower than that for the erratic boulder TM14-CS6. Apparent minimum ^{10}Be exposure ages are 0.70 ± 0.05, 0.53 ± 0.04, and 0.24 ± 0.02 Ma, and apparent steady-state erosion rates 0.81 ± 0.07, 1.12 ± 0.09, and 2.70 ± 0.19 m/Myr, respectively (Table 1). The sandstone and dolerite boulders comprising the lag deposit overlying the Sirius Group deposit at Table Mountain display surface varnish, and 1 cm wide pitting (Figures 3d and 3e), whereas the three cobble surfaces show little weathering, no pitting, and lack of siliceous crusts (Figures 3f and 4), likely due to the clasts being exhumed out of the Sirius Group deposit relatively recently (i.e., within the past ~1 million years).

When plotted on the ^{10}Be–^{26}Al/^{10}Be diagram, all these samples lie close to or inside the steady-state erosion island within their respective errors. The perched boulder lies within the steady-state erosion island, suggesting no

10.1029/2024JF007911

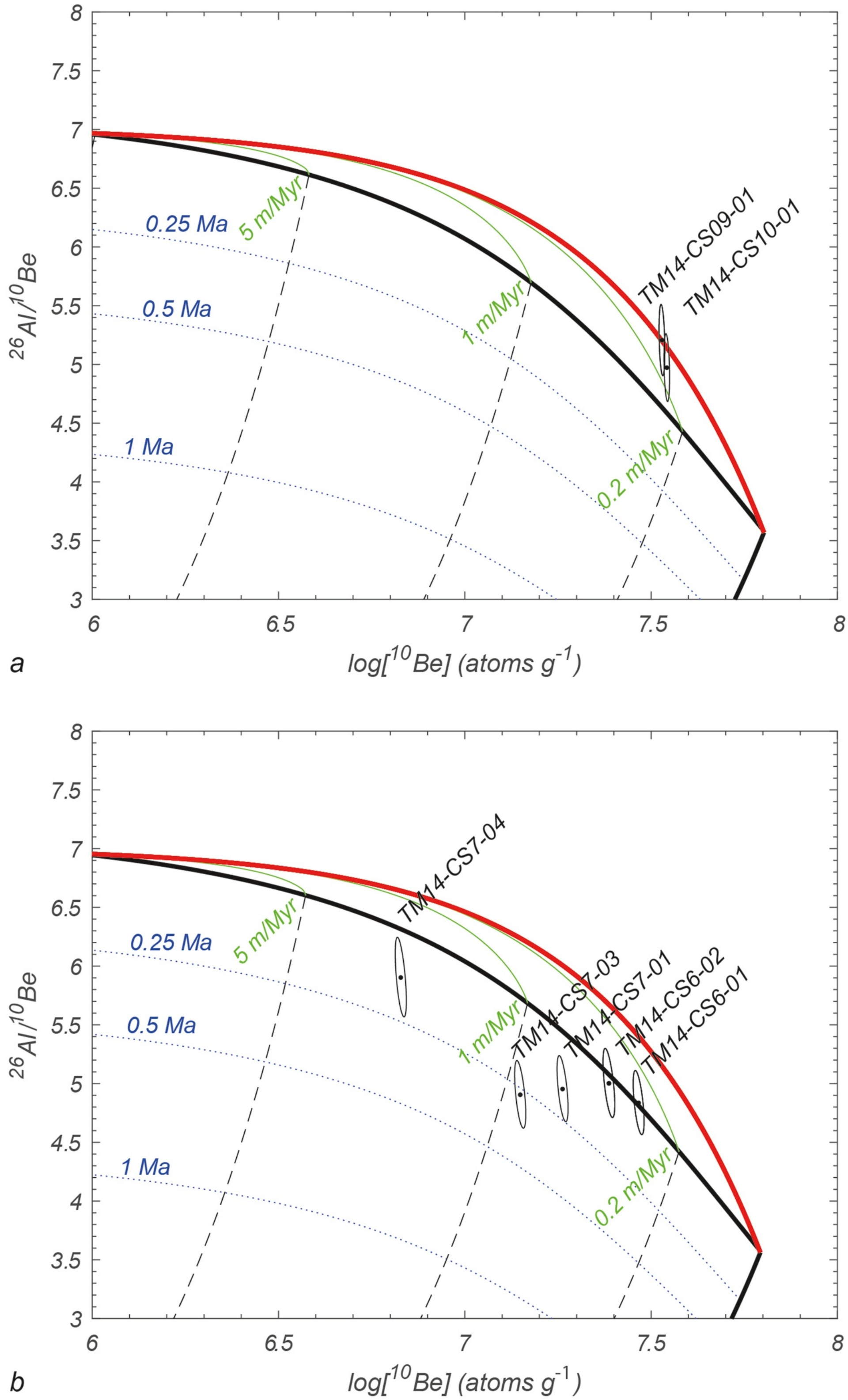

Figure 7. Two-isotope plots of (a) Table Mountain bedrock samples and (b) erratic boulder (TM14-CS6-01, −02) and embedded cobble samples (TM14-CS7-01, −03, −04). Measured nuclide concentrations with 1σ uncertainties. Burial isochrons (dotted lines), steady-state erosion loci (green lines), decay trajectories (dashed lines), and the erosion-exposure island (solid black and red lines) using the time-dependent "LSDn" scaling scheme of Lifton et al. (2014). The red line is the zero-erosion exposure line. The black line is the steady-state erosion line.

21699011, 2025, 3, Downloaded from https://agupubs.onlinelibrary.wiley.com/doi/10.1029/2024JF007911 by University Of Burgos, Wiley Online Library on [12/03/2026]. See the Terms and Conditions (https://onlinelibrary.wiley.com/terms-and-conditions) on Wiley Online Library for rules of use; OA articles are governed by the applicable Creative Commons License

10.1029/2024JF007911

21699011, 2025, 3, Downloaded from https://agupubs.onlinelibrary.wiley.com/doi/10.1029/2024JF007911 by University Of Burgos, Wiley Online Library on [12/03/2026]. See the Terms and Conditions (https://onlinelibrary.wiley.com/terms-and-conditions) on Wiley Online Library for rules of use; OA articles are governed by the applicable Creative Commons License

prior burial. The three embedded cobbles lie below the steady-state erosion island, indicating a complex burial-exposure history, totaling at most about ∼250 kyrs of burial, resulting from their exhumation to the surface of the permafrost sediment (Figure 7b).

4.2. Cosmogenic Nuclide Depth Profiles at Table Mountain

The ^{10}Be and ^{26}Al depth profiles from the permafrost core at Table Mountain are shown in Table 2 and Figure 6. The 20 ^{10}Be and 19 ^{26}Al concentrations from the depth profiles, ranging from 0.04 to 1.51 × 10^7 atoms g^{-1} of ^{10}Be and 0.23 to 8.76 × 10^7 atoms g^{-1} of ^{26}Al over the 2.95 m core length, show an exponential decay with depth (which is preserved when each sample depth is corrected for density changes reported in Table 2), suggesting there has been no significant vertical mixing or any post-depositional disturbance (Figure 6). This observation is also supported by a relatively uniform $^{26}Al/^{10}Be$ ratio (5.3–6.6). Based on our highest erosion rate of 2.7 m/Myr for the embedded cobble TM14-CS7-04, coupled with erosion rate constraints presented by Putkonen et al. (2008), we applied a maximum erosion limit of 400 cm for the depth profile modeling.

Our depth modeling simulations resulted in best-fits to measured ^{10}Be and ^{26}Al Sirius Group profiles for a surface erosion rate of $0.53^{+0.13}/_{-0.12}$ m/Myr, an exposure age of $0.78^{+0.06}/_{-0.08}$ Ma, and negligible inheritance (Figures 8 and 9). As presented for the subaerially exposed samples, we interpret the cosmogenic depth profile to reflect steady-state concentrations and take the modeled "exposure age" as a measure of the erosional time-scale whereby after 2–3 million years of exposure, production is balanced by decay and erosion resulting in equilibrium conditions and continual surface lowering at ∼0.53 m/Myr. Hence, denudation of the Sirius Group deposit results in exhumation of buried cobbles and boulders emerging as embedded material within the permafrost surface. The $^{26}Al/^{10}Be$ concentration ratio is broadly constant with depth for the entire core, showing an average value of ∼5.8 ± 0.3 (Table 2). When plotted on the ^{10}Be–$^{26}Al/^{10}Be$ diagram, the sample from the top of the depth profile (TM14-H-01) shows a simple exposure history plotting within the steady-state erosion island (Figure 10).

Our depth profile modeling cannot determine the true depositional age for the Sirius group. However, we note that best-fit model solutions resulted in zero values for both ^{10}Be and ^{26}Al inheritance in the core. This observation indicates that at the time of deposition, inheritance was either negligible, or that since deposition, the initial inheritance has decayed to a level indistinguishable from muogenic production. With respect to the measured ^{10}Be profile, taking the latter explanation as more likely, we can infer that inheritance today is negligible compared to the deepest ^{10}Be nuclide concentration of TM14-H-40 at 0.39 ± 0.01 × 10^6 atoms g^{-1} (see Table 2). We can thus use this observation to estimate a minimum deposition age of Sirius Group sediments at Table Mountain by assuming that the ^{10}Be concentration at deposition (i.e., the initial value of the inheritance) is represented by the mean ^{10}Be steady-state bedrock concentration of 3.4 × 10^7 atoms g^{-1} and the maximum inheritance observed today to be the lowest measured ^{10}Be value at the base of the core profile that is, 0.39 × 10^6 atoms g^{-1}. With a ^{10}Be half-life of 1.387 Ma (Chmeleff et al., 2010; Korschinek et al., 2010), the minimum deposition age is calculated to be ∼8.9 Ma. Based on our ^{10}Be depth profile data and the simple assumptions given above, we can provide a first-order estimate that the Sirius Group sediment was deposited more than 9 million years ago, largely consistent with the postulated middle Miocene age of the Sirius Group sediment given by Barrett and Powell (1982) and Goff et al. (2002). This estimate is also consistent with the onset of polar aridity, which Dickinson et al. (2012) inferred to have occurred more than 6 million years ago. Our results suggest that an initial non-zero inheritance is more likely than a zero inheritance, as the glaciofluvial and glaciolacustrine sediments at Table Mountain were deposited in a proglacial environment (Goff et al., 2002). In contrast, Shakun et al. (2018) found negligible initial in situ ^{10}Be in the ANDRILL core from a marine depositional environment, indicating that the sediments had minimal prior exposure. However, the ANDRILL core sediments were deposited by a large marine-based ice sheet that transported material from the Transantarctic Mountains into the Ross Embayment.

5. Discussion

Our data contributes to the existing cosmogenic nuclide inventory for high elevation, hyperarid landscapes in the Transantarctic Mountains, and when combined with other data sets, they provide valuable insight into the long-term geomorphic processes and past climate conditions of Antarctica. We compiled previously published cosmogenic nuclide data from Ivy-Ochs et al. (1995, 1997) and our own measurements from this study (Table 3). The samples are categorized into three groups: bedrock ($n = 2$, this study; $n = 9$, Ivy-Ochs et al., 1995), erratic boulders ($n = 1$, this study; $n = 1$, Ivy-Ochs et al., 1995), and embedded boulders and cobbles ($n = 2$, this study;

21699011, 2025, 3, Downloaded from https://agupubs.onlinelibrary.wiley.com/doi/10.1029/2024JF007911 by University Of Burgos, Wiley Online Library on [12/03/2026]. See the Terms and Conditions (https://onlinelibrary.wiley.com/terms-and-conditions) on Wiley Online Library for rules of use; OA articles are governed by the applicable Creative Commons License

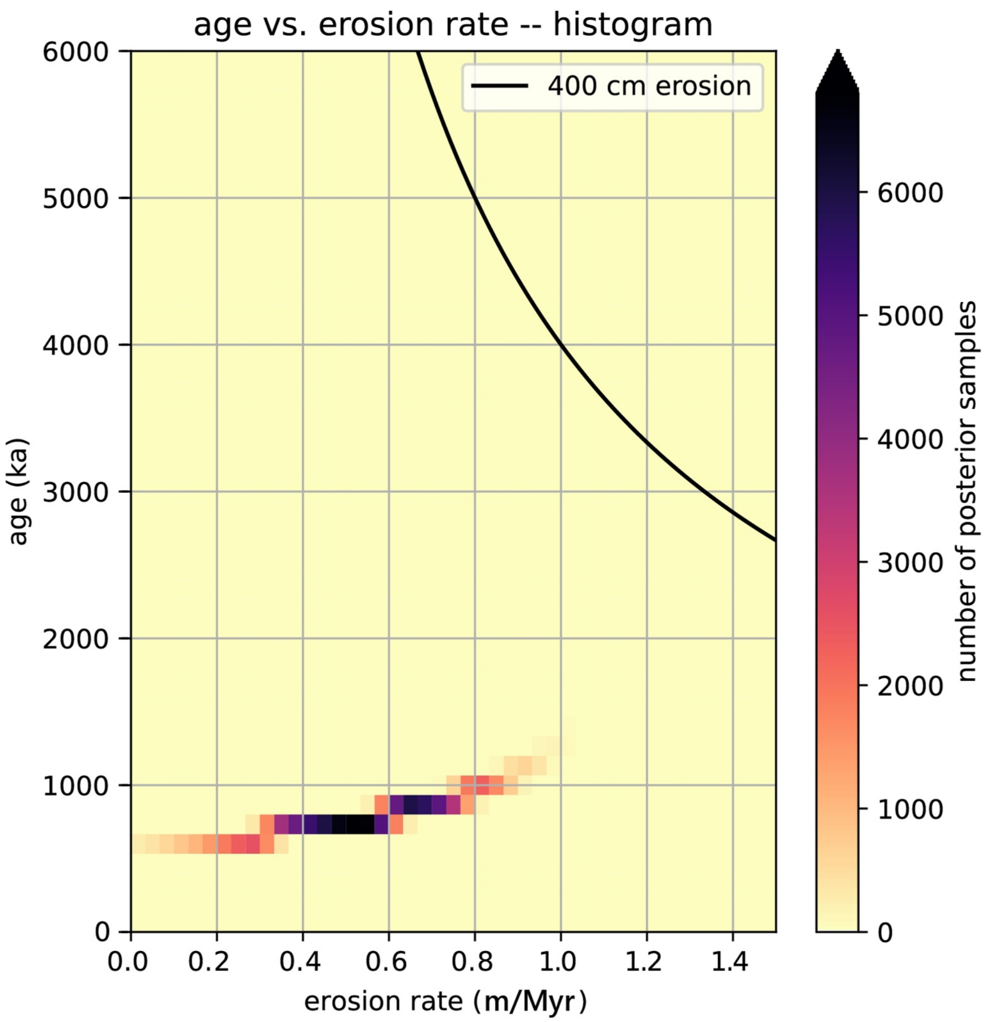

Figure 8. Age-erosion rate solution spaces using dual-nuclide depth profile modeling for TM14-H. The number of posterior samples refers to the quantity of data points from the depth profile modeling. Black line indicates 400 cm net erosion limit based on our highest erosion rate of 2.7 m/Myr for the embedded cobble TM14-CS7-04, and erosion rate constraints by Putkonen et al. (2008). Note that the solution space is not limited by the 400 cm net erosion limit.

n = 5, Ivy-Ochs et al., 1995); with respect to location and glacial geomorphology (see Figure 2, and Cox et al., 2012). Apparent exposure ages and steady-state erosion rates have been recalculated using version 3 of the CRONUS-Earth calculator (Balco et al., 2008), using the LSDn scaling scheme (Lifton et al., 2014) and the global mean calibration data set of Borchers et al. (2016). The erosion rates of the three groups are discussed in the following sections and compared in Figure 11. While snow cover is apparent in Figures 3 and 4, the hyperarid conditions, katabatic winds, and low air temperatures in the stable upland zone prevent long term accumulation of snow cover, and suggest that precipitation is unlikely to have a significant effect on the production of cosmogenic radionuclides due to shielding and thus on calculated erosion rates (Marrero et al., 2018).

5.1. Erosion Constraints for Plateau Surface Bedrock

The ^{10}Be measurements from 11 sandstone bedrock samples at Table Mountain ($n = 2$, this study; $n = 9$, Ivy-Ochs et al., 1995) give apparent erosion rates ranging from 0.04–0.39 m/Myr with a mean of 0.17 ± 0.12 m/Myr (Table 3; Figure 2). The ^{10}Be–^{26}Al/^{10}Be diagram shows that the bedrock surfaces from our study have had continuous exposure and steady erosion for at least 1.6 Ma (Figure 7a). Our results are consistent with the recalculated bedrock erosion rates in Ivy-Ochs et al. (1995, 1997) that indicate that during the past 3 million years, a maximum of ~1 m of sandstone has been eroded from the plateau surface at Table Mountain. These ^{10}Be

10.1029/2024JF007911

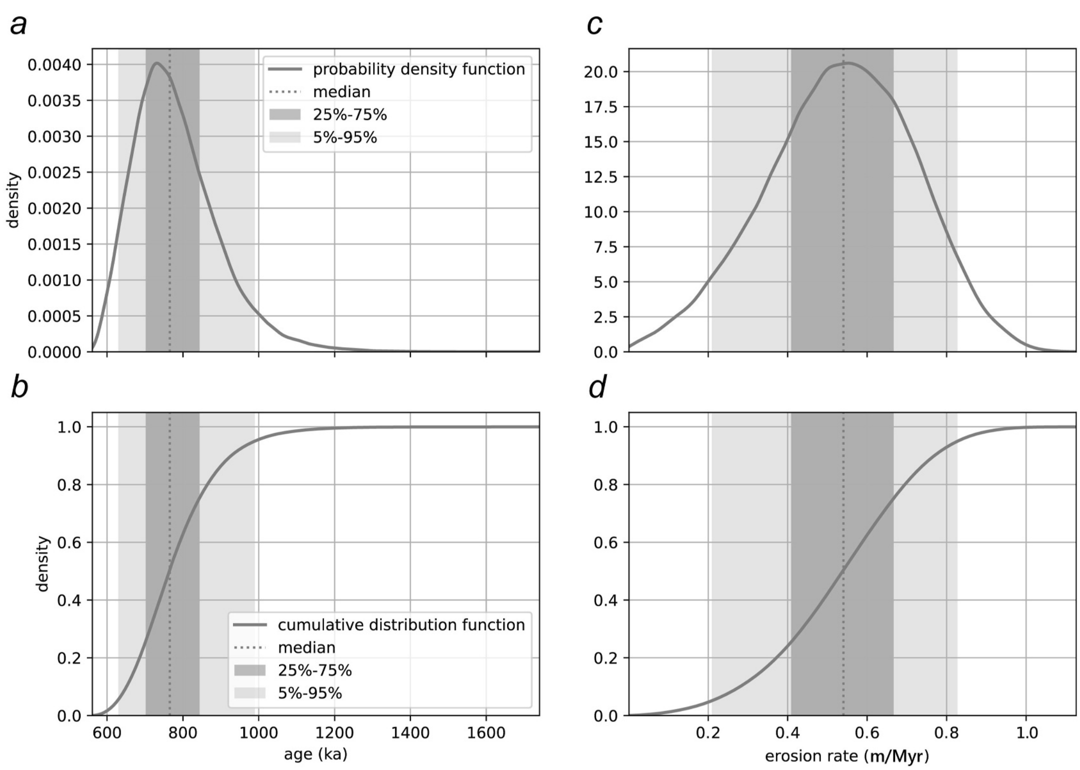

Figure 9. Probability density function, and cumulative distribution function for (a, b) exposure age (ka) and (c, d) apparent erosion rate (m/Myr) using dual-nuclide depth profile modeling resulting from 100,000 iterations to simulate the measured ^{10}Be and ^{26}Al TM14-H concentrations.

erosion rates are also consistent with those measured on bedrock surfaces at other high elevation McMurdo Dry Valley sites (e.g., Balco et al., 2014), but are not as low as sandstone erratics at southern Transantarctic Mountain sites with erosion rates between 0.005–0.03 m/Myr from paired ^{10}Be–^{21}Ne measurements (Balter-Kennedy et al., 2020). The higher erosion rates in the McMurdo Dry Valleys area may be due to a greater sediment supply (Marrero et al., 2018), which could have acted as an abrasion agent of enhanced physical weathering compared to regions largely covered by ice.

5.2. Erosion Constraints and Landscape Evolution for Overlying Erratic Boulder and Cobbles Embedded in Sirius Group Sediments

As the deposition age of the Sirius Group sediment is stratigraphically considered middle Miocene, which in this work is largely supported by the minimum age estimate from our depth profile data (cf. Section 4.2), we interpret the cosmogenic nuclide data for erratics and embedded cobbles, resulting from the exhumation process and subsequent subaerial exposure, as time-averaged erosion rates.

^{10}Be and ^{26}Al data from two erratic boulders, sample 205 from Ivy-Ochs et al. (1995) collected at the margin of the debris flow and on Ferrar Dolerite bedrock (see Figure 2) and from TM14-CS6 overlying the Sirius Group, give steady-state ^{10}Be erosion rates of 0.14 ± 0.04 and 0.42 ± 0.03 m/Myr with a mean of 0.28 ± 0.20 m/Myr (Table 3). The five granite embedded cobble samples (207, 208, 209, 217a, 217b) measured by Ivy-Ochs et al. (1995) were collected from the debris flow sediments downslope on the margin of the Sirius Group (Figure 2). Together with our two embedded cobbles (TM14-CS7-01 and −03), this group gives a mean apparent steady-state ^{10}Be erosion rate of 0.59 ± 0.36 m/Myr. We note that the third sandstone cobble embedded in the Sirius Group, TM14-CS7-04, gives a significantly higher ^{10}Be (and ^{26}Al) erosion rate of 2.70 ± 0.19 m/Myr. Barring any unaccounted analytical error, the erosion-exposure history for this sample differs considerably from all other samples at this site. This result may be consistent with the continuous process of Sirius Group exhumation and represent a more recent subaerial exposure, though other effects such as thick cover by a layer of clasts or similar cannot be discounted. For comparison purposes of mean erosion rates, we have chosen not to include it in the average for this group.

21699011, 2025, 3, Downloaded from https://agupubs.onlinelibrary.wiley.com/doi/10.1029/2024JF007911 by University Of Burgos, Wiley Online Library on [12/03/2026]. See the Terms and Conditions (https://onlinelibrary.wiley.com/terms-and-conditions) on Wiley Online Library for rules of use; OA articles are governed by the applicable Creative Commons License

21699011, 2025, 3, Downloaded from https://agupubs.onlinelibrary.wiley.com/doi/10.1029/2024JF007911 by University Of Burgos, Wiley Online Library on [12/03/2026]. See the Terms and Conditions (https://onlinelibrary.wiley.com/terms-and-conditions) on Wiley Online Library for rules of use; OA articles are governed by the applicable Creative Commons License

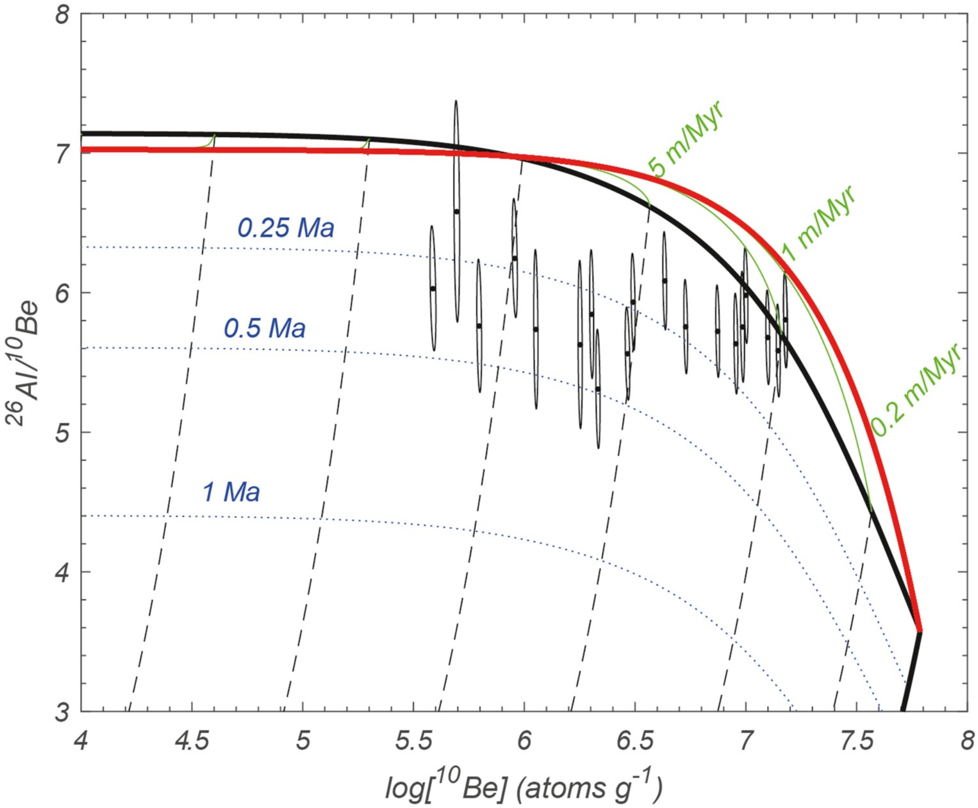

Figure 10. Two-isotope plot of TM14-H permafrost depth profile measurements. Nuclide concentrations are plotted with 1σ uncertainties, using the time-dependent "LSDn" scaling scheme of Lifton et al. (2014), burial isochrons (dotted lines), steady-state erosion loci (green lines), decay trajectories (dashed lines), and the erosion-exposure island (solid black and red lines). The red line is the zero-erosion exposure line. The black line is the steady-state erosion line.

The mean erosion rate for the embedded clasts was higher (0.59 ± 0.36 m/Myr) than the free-standing erratics (0.28 ± 0.20 m/Myr). Given the large spread in maximum erosion rates of both groups, it would be reasonable to conclude that these samples may have experienced similar, or only slightly different, exposure-erosion histories. However, bedrock ^{10}Be erosion rates range from 0.04 to 0.39 m/Myr with a mean of 0.17 ± 0.12 m/Myr, that is distinctly lower by a factor of three than the mean value for embedded cobbles. Despite this large difference in average value, the 1 sigma relative standard deviation for these three groups are all rather large, of the order of 61%–73%, resulting in some overlap in the population of individual sample erosion rates (which ranges from 0.04 to 1.1 m/Myr). This observation is consistent with the formation of a dynamic surface layer erosional lag deposit.

There were striking differences in surface weathering characteristics between the three groups of samples. Of the nine sandstone bedrock samples reported by Ivy-Ochs et al. (1995), five of them have silicified surfaces (see Table 3). Sample TM14-CS6, from the overlying erosional lag formation, and sample 205 reported by Ivy-Ochs et al. (1995), perched on the Ferrar Dolerite bedrock surface, also show a similar well-developed surface desert varnish cover. None of the eight embedded cobbles in the Sirius Group exhibit silicified surface armoring or desert varnish, suggesting that the resistant oxide coating created during prolonged subaerial exposure protects the bedrock and erratic surfaces from enhanced weathering. The variability of sandstone erosion rates across Antarctica has also been attributed to the degree of desert varnish (Marrero et al., 2018). At Table Mountain, boulders and cobbles are continuously being exhumed from the Siris Group sediments on to the surface. Our erosion rates from erratic boulders and embedded cobbles are higher than the neighboring plateau bedrock surfaces. These data differ from the broader pattern of compiled erosion rates of sandstone surfaces across Antarctica, where boulders yield lower erosion rates than collected bedrock surfaces (Marrero et al., 2018). We attribute our higher boulder and embedded cobble erosion rates compared to our bedrock data to exhumation processes that affect the subaerial exposure history and development of desert varnish.

Table 3
Minimum Exposure Ages and Apparent Erosion Rates for Table Mountain From This Study and Ivy-Ochs et al. (1995)

Sample name[a]	Sample description[b]	^{10}Be age (Ma)	^{10}Be erosion rate (m/Myr)	^{26}Al age (Ma)	^{26}Al erosion rate (m/Myr)
Bedrock					
I1995-213a and 213a-R	Sandstone cobble from TGPS	3.01 ± 0.43	0.09 ± 0.01	–	–
I1995-214b	Silicified sandstone cobble from TGPS	3.31 ± 0.67	0.07 ± 0.03	1.28 ± 0.28	0.23 ± 0.09
I1995-218 and 218-R	TGPS sandstone bedrock	1.15 ± 0.12	0.39 ± 0.05	0.74 ± 0.11	0.55 ± 0.11
I1995-219a	Sandstone cobble from TGPS	1.37 ± 0.18	0.30 ± 0.06	1.03 ± 0.24	0.33 ± 0.13
I1995-219b	Sandstone cobble from TGPS	1.87 ± 0.25	0.19 ± 0.04	–	–
I1995-220	Silicified sandstone bedrock from TGPS	4.09 ± 1.24	0.04 ± 0.03	1.85 ± 0.53	0.11 ± 0.07
I1995-323	Silicified sandstone bedrock from TGPS	3.68 ± 0.83	0.06 ± 0.03	1.44 ± 0.45	0.19 ± 0.11
I1995-325	Silicified sandstone bedrock from TGPS	2.43 ± 0.43	0.13 ± 0.04	–	–
I1995-326	Silicified sandstone bedrock from TGPS	4.12 ± 1.12	0.04 ± 0.03	–	–
TM14-CS09-01	Sandstone bedrock from TGPS	1.57 ± 0.14	0.28 ± 0.04	1.58 ± 0.36	0.18 ± 0.08
TM14-CS10-01	Sandstone bedrock from TGPS	1.67 ± 0.16	0.26 ± 0.04	1.55 ± 0.35	0.18 ± 0.08
Average:		**2.57 ± 1.12 (43%) (n = 11)**	**0.17 ± 0.12 (73%) (n = 11)**	**1.35 ± 0.37 (27%) (n = 7)**	**0.25 ± 0.15 (58%) (n = 7)**
Erratic boulders					
I1995-205	Silicified sandstone on dolerite surface	2.34 ± 0.37	0.14 ± 0.04	1.33 ± 0.29	0.22 ± 0.09
TM14-CS6-01 + 6−02	*Exhumed sandstone boulder on SG*	1.09 ± 0.07	0.42 ± 0.03	0.89 ± 0.10	0.43 ± 0.07
Average:		**1.72 ± 0.88 (51%) (n = 2)**	**0.28 ± 0.20 (72%) (n = 2)**	**1.11 ± 0.31 (28%) (n = 2)**	**0.32 ± 0.15 (46%) (n = 2)**
Embedded boulders and cobbles					
I1995-207 + 207-R	Granite cobble in SG	1.27 ± 0.15	0.34 ± 0.05	0.69 ± 0.08	0.59 ± 0.09
I1995-208	Granite cobble in SG	0.84 ± 0.09	0.58 ± 0.07	0.53 ± 0.07	0.85 ± 0.15
I1995-209 + 209-R	Granite cobble in SG	0.60 ± 0.07	0.85 ± 0.11	0.38 ± 0.03	1.29 ± 0.14
I1995-217a	Granite boulder in SG	1.57 ± 0.19	0.25 ± 0.04	1.12 ± 0.21	0.29 ± 0.09
I1995-217b	Granite boulder in SG	2.08 ± 0.42	0.16 ± 0.05	1.16 ± 0.23	0.28 ± 0.09
TM14-CS7-01	*Sandstone cobble in SG*	0.70 ± 0.05	0.81 ± 0.07	0.54 ± 0.06	0.95 ± 0.15
TM14-CS7-03	*Sandstone cobble in SG*	0.53 ± 0.04	1.12 ± 0.09	0.39 ± 0.04	1.42 ± 0.19
TM14-CS7-04[c]	*Sandstone cobble in SG*	(0.24 ± 0.02)	(2.70 ± 0.19)	(0.21 ± 0.02)	(2.93 ± 0.33)
Average:		**1.08 ± 0.59 (54%) (n = 7)**	**0.59 ± 0.36 (61%) (n = 7)**	**0.69 ± 0.32 (47%) (n = 7)**	**0.81 ± 0.45 (56%) (n = 7)**

Note. All data from Ivy-Ochs et al. (1995, 1997) are derived from ICE-D (recalculated using revised values for AMS standards referenced to 07KNSTD series). Minimum exposure ages and maximum erosion rates were calculated using Version 3 of CRONUS-Earth and the LSDn Scaling Scheme (Lifton et al., 2014) and the primary calibration data set of Borchers et al. (2016). All errors are external uncertainties given by the CRONUS-Earth calculator. [a]All samples labeled with prefix I1995 are from Ivy-Ochs et al. (1995) and Ivy-Ochs et al. (1997). Samples ending in "-R" are duplicates and final data (in bold) are given as a weighted mean and standard mean error (standard deviation and relative standard deviation). All sample names in italics are from this study. [b]TGPS, Taylor Group (Beacon Supergroup) Plateau surface. SG, Sirius Group. See Figure 2. [c]Sample TM-CS7-04 has been rejected as an outlier for calculation of group average values.

5.3. Permafrost Stability at Table Mountain

We interpret the $0.53^{+0.13}/_{-0.12}$ m/Myr erosion rate derived from modeling the TM14-H depth profile as the long-term surface denudation rate of the Sirius Group sediments, allowing embedded boulders and cobbles to be continuously exhumed and concentrated on the surface, and then forming the observed erosional lag formation (Figure 12). The exhumed sandstone cobbles and boulders may not have had similar initial cosmogenic concentrations, but once fully exhumed, they will experience similar subaerial weathering processes. The increase in production rate once fully exhumed, would result in sample-specific erosion rates we have quantified in erratic boulders and the embedded cobbles, that would contrast with steady-state continuously exposed bedrock surfaces

21699011, 2025, 3, Downloaded from https://agupubs.onlinelibrary.wiley.com/doi/10.1029/2024JF007911 by University Of Burgos, Wiley Online Library on [12/03/2026]. See the Terms and Conditions (https://onlinelibrary.wiley.com/terms-and-conditions) on Wiley Online Library for rules of use; OA articles are governed by the applicable Creative Commons License

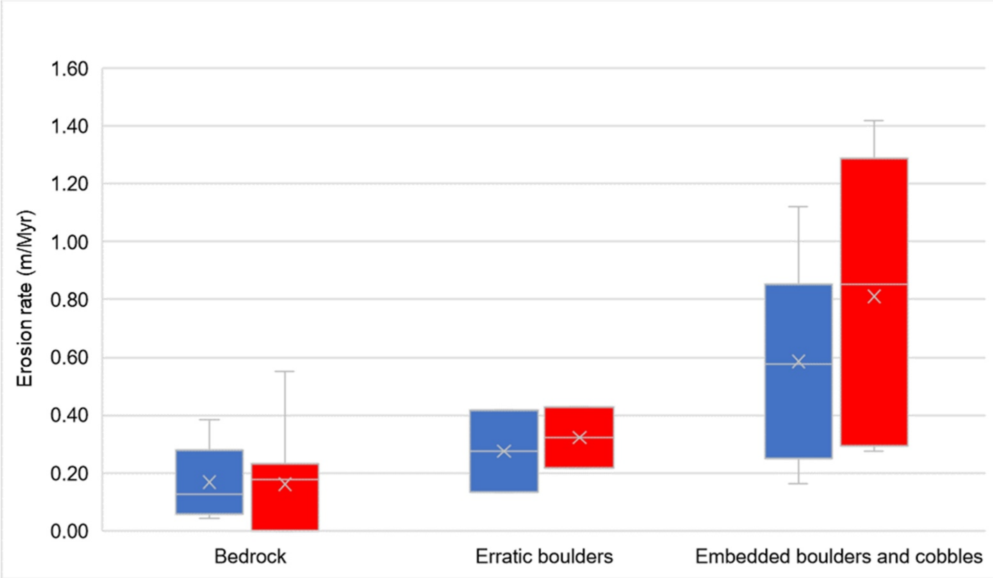

Figure 11. ^{10}Be (blue) and ^{26}Al (red) derived erosion rates of bedrock, erratic boulders, and embedded boulders and cobbles at Table Mountain. Erosion rates were calculated from previously published cosmogenic nuclide data (Ivy-Ochs et al., 1995, 1997) and our own measurements from this study.

(see Table 3). The modeled surface erosion rate for the Sirius Group profile of $0.53^{+0.13}/_{-0.12}$ m/Myr is consistent with the mean ^{10}Be erosion rate for the embedded boulders and cobbles (0.59 ± 0.36 m/Myr; $n = 7$), suggesting that, on average, the embedded boulders and cobbles have undergone the same burial-exposure history as the Sirius Group sediments. The large range in the weathering rates of the embedded group most likely reflects differences in their exposure time since exhumation, and/or other subaerial processes (e.g., local shielding, sediment, and snow cover).

The ^{10}Be and ^{26}Al depth profiles from the TM14-H permafrost core show no sign of mixing, ice sublimation, or any other post-depositional disturbance (Figure 6). These data suggest that the clean ice lenses below the ice table (between 0.47–0.75 m depth) have been stable, or in equilibrium (between loss and recharging) for at least ~2–3 million years, representing the time required to achieve steady-state depth profile conditions based on our model surface erosion rate of 0.53 m/Myr. We suggest that the accumulation of ice from 0.47 m depth, reflects a paleosublimation unconformity, and corresponds with the maximum predicted ice-table depth (Lapalme et al., 2017). Paleosublimation unconformities are typical of permafrost in the stable upland zone, and have also been observed in University Valley, ~30 km west of Table Mountain (Lapalme et al., 2017). While sublimation can occur above the ice-table depth, ground ice below this depth will continue to accumulate over time via atmospheric water vapor and brine film recharge (Dickinson & Rosen, 2003). Ice table migration and ice recharging processes may have occurred for more than 6 Ma (Dickinson et al., 2012).

5.4. Implications for Erosion Rate Constraints

The ^{10}Be and ^{26}Al nuclide concentrations from Beacon sandstone bedrock, boulder surfaces within the erosional lag formation, and embedded cobbles within the Sirius Group surface are all best interpreted as apparent erosion rates that range from ~0.04–1.1 m/Myr. These erosion rates are consistent with other studies of similar exposed bedrock, boulders and cobbles that have likely been exposed since at least the late Miocene. The model erosion rate derived from underlying Sirius Group depth profiles of 0.53 m/Myr is best interpreted as the steady-state surface denudation rate and, in general, is higher than the mean erosion rate of the overlying erosional lag formation and nearby bedrock surfaces. Our Sirius Group denudation rate at Table Mountain is broadly in agreement with previously reported erosion rates from high elevation regolith in the Transantarctic Mountains ranging between 0.19–2.1 m/Myr (Bergelin et al., 2022; Bibby et al., 2016; Morgan et al., 2010, 2011; Putkonen et al., 2008). However, in contrast, these rock surface weathering and in situ depth profile Sirius Group denudation rates are about an order of magnitude (or more) greater than the extremely low erosion rates of 0.01–0.06 m/Myr derived from infiltration of meteoric ^{10}Be in Sirius Group sediments at Table Mountain calculated by

21699011, 2025, 3, Downloaded from https://agupubs.onlinelibrary.wiley.com/doi/10.1029/2024JF007911 by University Of Burgos, Wiley Online Library on [12/03/2026]. See the Terms and Conditions (https://onlinelibrary.wiley.com/terms-and-conditions) on Wiley Online Library for rules of use; OA articles are governed by the applicable Creative Commons License

21699011, 2025, 3, Downloaded from https://agupubs.onlinelibrary.wiley.com/doi/10.1029/2024JF007911 by University Of Burgos, Wiley Online Library on [12/03/2026]. See the Terms and Conditions (https://onlinelibrary.wiley.com/terms-and-conditions) on Wiley Online Library for rules of use; OA articles are governed by the applicable Creative Commons License

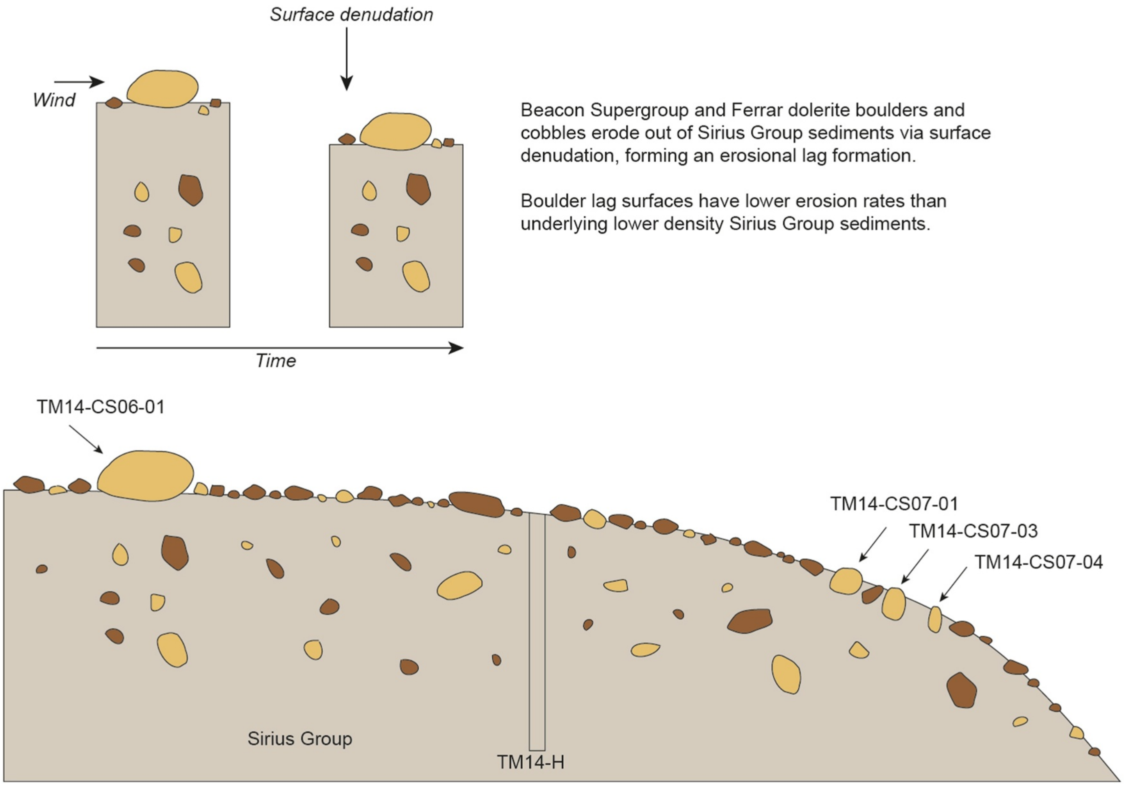

Figure 12. Schematic diagram of Table Mountain landscape showing Sirius Group and formation of boulder and cobble lag. Beacon sandstone boulder sample (TM14-CS6-01), and embedded cobble samples.

Dickinson et al. (2012) and Verret et al. (2023). Dickinson et al. (2012) argued that the difference in erosion rates between their TM1 and TM4 drill sites may be explained by a shielding effect of the erosional lag deposit of dolerite and sandstone clasts compared to lower density friable underlying Sirius Group sediments. The TM1 site was covered by a desert pavement, the sample was collected from the debris flow deposit, and gave a low erosion rate of 0.02 m/Myr. The TM4 site had little desert pavement, the sample was collected from the Sirius Group sediment, and gave a comparatively high erosion rate of 0.06 m/Myr. Their field observations and meteoric ^{10}Be-based erosion rates from TM1 and TM4 may well be consistent, but the magnitude of the meteoric ^{10}Be erosion rate is inconsistent with our in situ ^{10}Be- and ^{26}Al- based erosion rates for the Sirius Group depth profile. The abundance of Ferrar Dolerite and Beacon sandstone clasts overlying the Sirius Group sediments at our coring site highlights the low resistance to erosion and transport of the low density, friable Sirius Group (Figures 3 and 4). Based on this observation, the erosion rate of 0.06 m/Myr at TM4 appears unusually low, where there is no desert lag. Alternatively, the lack of desert lag at TM4 may also be explained at a low erosion rate that prevents clasts from being exhumed. We acknowledge that small variations in topography and orientation can have large impacts on denudation, and may explain the difference in erosion rates between sites TM1, TM4 and TM14-H. However, cosmogenic-nuclide derived erosion rates are time-averaged and do not necessarily reflect the current erosion rate or present-day geomorphology. As such, the difference may also reflect temporal changes in erosion rates from the late Miocene to the Plio-Pleistocene. It is important in this comparison of erosion rates between cores to keep in mind that the resultant ^{10}Be depth profiles of TM1 and TM4 are based on modeling the mobility of atmospheric deposited meteoric ^{10}Be, and TM14-H is based on in situ production of ^{10}Be in quartz grains. These two approaches are based on very different processes that are constrained by specific assumptions and conditions. Further clarification and additional data are required to resolve such discrepancies between the in situ ^{10}Be-based erosion rates and meteoric ^{10}Be-based erosion rates. Nonetheless, this study illustrates that surface strata and sediments with varying protection from surface lag deposits, can have significant implications on landscape evolution, with erosion rates differing by several meters over a few million years.

21699011, 2025, 3, Downloaded from https://agupubs.onlinelibrary.wiley.com/doi/10.1029/2024JF007911 by University Of Burgos, Wiley Online Library on [12/03/2026]. See the Terms and Conditions (https://onlinelibrary.wiley.com/terms-and-conditions) on Wiley Online Library for rules of use; OA articles are governed by the applicable Creative Commons License

6. Conclusions

At Table Mountain in the Transantarctic Mountains, we measured ^{10}Be and ^{26}Al nuclide concentrations from bedrock, erratic boulders, and cobbles embedded in Sirius Group surface sediments, and from a 2.95 m depth profile through underlying Sirius Group sediments to constrain and compare surface erosion rates from various landforms in one of the coldest, driest regions on Earth.

Measured ^{10}Be and ^{26}Al concentrations in this study, together with previously published data from plateau surface sandstone bedrock, are best explained by apparent erosion rates of 0.04–0.55 m/Myr, with a mean apparent ^{10}Be bedrock erosion rate of 0.17 ± 0.12 m/Myr ($n = 11$). Erosion rates for clasts embedded within the Sirius Group range between 0.16–1.12 m/Myr, with a mean ^{10}Be erosion rate of 0.59 ± 0.36 m/Myr ($n = 7$) being three times larger than that for bedrock surfaces. Within the lag deposit overlying the Sirius Group and immediately outside and below the debris flow, we find ^{10}Be and ^{26}Al concentrations from two sandstone erratic boulders are best explained by apparent erosion rates of 0.14–0.43 m/Myr, with a mean ^{10}Be erosion rate of 0.28 ± 0.20 m/Myr. Both bedrock and erratics exhibit significant desert vanish, which tends to armor the eroding surfaces and hence reduce weathering.

Depth profile modeling of the sediment core through the Sirius Group deposit provides a best fit to the measured ^{10}Be and ^{26}Al concentrations with a steady-state erosion rate of $0.53^{+0.13}/_{-0.12}$ m/Myr, and an erosional-time scale of $0.78^{+0.06}/_{-0.08}$ Ma, the latter representing the time to denude one cosmic ray attenuation length of production in Sirius Group surface sediments to maintain steady-state equilibrium conditions. This result implies a certain degree of permafrost and climate stability at Table Mountain for ∼2–3 million years. The denudation rate of Sirius Group sediments is, on average, similar to the mean surface erosion rate of its embedded cobbles. Deflation of the Sirius Group surface deposit results in exhumation of buried cobbles and boulders emerging as embedded material which accumulate on the permafrost surface forming an erosional lag deposit. These materials undergo increased subaerial production and subsequently reach steady-state conditions. Our depth profile modeling of ^{10}Be and ^{26}Al concentrations indicates that most if not all inheritance has decayed or is insignificant compared to post-deposition production down the core. Taking the mean bedrock ^{10}Be concentration and the ^{10}Be concentration from the deepest profile sample to represent initial ^{10}Be at deposition, and final ^{10}Be at time of collection, respectively, we estimate a 9 Ma minimum deposition age for the Sirius Group–a result largely consistent with the postulated middle Miocene age of the Sirius Group at Table Mountain.

Together with other in situ-based erosion rates from high elevation regolith in the Transantarctic Mountains, our erosion rates are not consistent – on average up to an order of magnitude different – with previously reported extremely low erosion rates of 0.01–0.06 m/Myr derived from meteoric ^{10}Be measurements in Sirius Group sediments at Table Mountain. Discrepancies between the calculated in situ ^{10}Be erosion rates and meteoric ^{10}Be erosion rates require further clarification.

Data Availability Statement

Analytical data for all ^{10}Be and ^{26}Al measurements are available in Anderson et al. (2025). Data for surface samples are archived on the ICE-D Antarctica database (https://www.ice-d.org/antarctica/site/TABLE/).

Acknowledgments
We thank the late Craig Cary, Ian McDonald, Bob Dagg and Steph Lambie for assistance in the field, Antarctica New Zealand and Southern Lakes Helicopters for logistical support, and Steve Kotevski for laboratory assistance. We dedicate this paper to the memory of Craig Cary. *Financial Support:* This research was supported by NZARI (RFP 2014-1), and ANSTO Portal Grants 12215 and 12260 and an AINSE Postgraduate Research Award. JTHA was supported by a Sir Robin Irvine Scholarship, and a University of Otago departmental award. AA and ND were partially supported by the Russian Antarctic Expedition. We acknowledge the financial support from the Australian Government for the Centre for Accelerator Science at ANSTO through the National Collaborative Research Infrastructure Strategy (NCRIS). Prepared in part by LLNL under Contract DE-AC52-07NA27344 and LDRD Grant 19-LW-036. This is LLNL-JRNL-842939. Open access publishing facilitated by University of Otago, as part of the Wiley - University of Otago agreement via the Council of Australian University Librarians.

References

Anderson, J. T. H., Fink, D., Fujioka, T., Hidy, A., Wilson, G. S., Abramov, A., et al. (2025). Constraining erosion rates and landscape evolution with ^{10}Be and ^{26}Al cosmogenic nuclides at Table Mountain, Antarctica [Dataset]. *Journal of Geophysical Research: Earth Surface*. https://doi.org/10.6084/m9.figshare.28352696.v1

Anderson, J. T. H., Fujioka, T., Fink, D., Hidy, A. J., Wilson, G. S., Wilcken, K., et al. (2023). Antarctic permafrost processes and antiphase dynamics of cold-based glaciers in the McMurdo Dry Valleys inferred from ^{10}Be and ^{26}Al cosmogenic nuclides. *The Cryosphere Discussions*, *17*(11), 4917–4936. https://doi.org/10.5194/tc-17-4917-2023

Anderson, R. S., Repka, J. L., & Dick, G. S. (1996). Explicit treatment of inheritance in dating depositional surfaces using in situ ^{10}Be and ^{26}Al. *Geology*, *24*(1), 47–51. https://doi.org/10.1130/0091-7613(1996)024<0047:ETOIID>2.3.CO;2

Balco, G. (2017). Production rate calculations for cosmic-ray-muon-produced ^{10}Be and ^{26}Al benchmarked against geological calibration data. *Quaternary Geochronology*, *39*, 150–173. https://doi.org/10.1016/j.quageo.2017.02.001

Balco, G., Blard, P. H., Shuster, D. L., Stone, J. O. H., & Zimmermann, L. (2019). Cosmogenic and nucleogenic ^{21}Ne in quartz in a 28-meter sandstone core from the McMurdo Dry Valleys, Antarctica. *Quaternary Geochronology*, *52*, 63–76. https://doi.org/10.1016/j.quageo.2019.02.006

Balco, G., Stone, J. O., Lifton, N. A., & Dunai, T. J. (2008). A complete and easily accessible means of calculating surface exposure ages or erosion rates from ^{10}Be and ^{26}Al measurements. *Quaternary Geochronology*, *3*(3), 174–195. https://doi.org/10.1016/j.quageo.2007.12.001

21699011, 2025, 3, Downloaded from https://agupubs.onlinelibrary.wiley.com/doi/10.1029/2024JF007911 by University Of Burgos, Wiley Online Library on [12/03/2026]. See the Terms and Conditions (https://onlinelibrary.wiley.com/terms-and-conditions) on Wiley Online Library for rules of use; OA articles are governed by the applicable Creative Commons License

Balco, G., Stone, J. O. H., Sliwinski, M. G., & Todd, C. (2014). Features of the glacial history of the Transantarctic Mountains inferred from cosmogenic ^{26}Al, ^{10}Be and ^{21}Ne concentrations in bedrock surfaces. *Antarctic Science*, *26*(6), 708–723. https://doi.org/10.1017/S0954102014000261

Balter-Kennedy, A., Bromley, G., Balco, G., Thomas, H., & Jackson, M. S. (2020). A 14.5-million-year record of East Antarctic ice sheet fluctuations from the central transantarctic Mountains, constrained with cosmogenic ^{3}He, ^{10}Be, ^{21}Ne, and ^{26}Al. *The Cryosphere*, *14*(8), 2647–2672. https://doi.org/10.5194/tc-14-2647-2020

Barrett, P. J., & Powell, R. D. (1982). Middle cenozoic glacial beds at Table Mountain, southern victoria land. *Antarctic geoscience*, 1059–1067.

Bergelin, M., Putkonen, J., Balco, G., Morgan, D., Corbett, L. B., & Bierman, P. R. (2022). Cosmogenic nuclide dating of two stacked ice masses: Ong Valley, Antarctica. *The Cryosphere*, *16*(7), 2793–2817. https://doi.org/10.5194/tc-16-2793-2022

Bibby, T., Putkonen, J., Morgan, D., Balco, G., & Shuster, D. L. (2016). Million year old ice found under meter thick debris layer in Antarctica. *Geophysical Research Letters*, *43*(13), 6995–7001. https://doi.org/10.1002/2016GL069889

Borchers, B., Marrero, S., Balco, G., Caffee, M., Goehring, B., Lifton, N., et al. (2016). Geological calibration of spallation production rates in the CRONUS-Earth project. *Quaternary Geochronology*, *31*, 188–198. https://doi.org/10.1016/j.quageo.2015.01.009

Bruno, L. A., Baur, H., Graf, T., Schlüchter, C., Signer, P., & Wieler, R. (1997). Dating of sirius group tillites in the Antarctic dry valleys with cosmogenic ^{3}He and ^{21}Ne. *Earth and Planetary Science Letters*, *147*(1–4), 37–54. https://doi.org/10.1016/s0012-821x(97)00003-4

Chmeleff, J., von Blanckenburg, F., Kossert, K., & Jakob, D. (2010). Determination of the ^{10}Be half-life by multicollector ICP-MS and liquid scintillation counting. *Nuclear Instruments and Methods in Physics Research Section B: Beam Interactions with Materials and Atoms*, *268*(2), 192–199. https://doi.org/10.1016/j.nimb.2009.09.012

Chorley, H., Levy, R., Naish, T., Lewis, A., Cox, S., Hemming, S., et al. (2023). East Antarctic ice sheet variability during the middle Miocene climate transition captured in drill cores from the Friis Hills, transantarctic Mountains. *GSA Bulletin*, *135*(5–6), 1503–1529. https://doi.org/10.1130/B36531.1

Cox, S. C., Turnbull, I. M., Isaac, M. J., Townsend, D. B., & Smith Lyttle, B. (2012). Geology of southern victoria land, Antarctica. In *Institute of geological & Nuclear Sciences 1:25,000 geological map 22. 135 p. + 1 folded map*. GNS Science.

Dickinson, W. W., & Rosen, M. R. (2003). Antarctic permafrost: An analogue for water and diagenetic minerals on Mars. *Geology*, *31*(3), 199–202. https://doi.org/10.1130/0091-7613(2003)031<0199:APAAFW>2.0.CO;2

Dickinson, W. W., Schiller, M., Ditchburn, B. G., Graham, I. J., & Zondervan, A. (2012). Meteoric Be-10 from Sirius Group suggests high elevation McMurdo Dry Valleys permanently frozen since 6Ma. *Earth and Planetary Science Letters*, *355–356*, 13–19. https://doi.org/10.1016/j.epsl.2012.09.003

Fielding, C. R., Harwood, D. M., Winter, D. M., & Francis, J. E. (2012). Neogene stratigraphy of Taylor valley, transantarctic Mountains, Antarctica: Evidence for climate dynamism and a vegetated early Pliocene coastline of McMurdo sound. *Global and Planetary Change*, *96–97*, 97–104. https://doi.org/10.1016/j.gloplacha.2010.09.003

Goff, J. R., Jennings, I. W., & Dickinson, W. W. (2002). Depositional environment of sirius group sediments, Table Mountain, Dry Valleys area, Antarctica. *Geografiska Annaler—Series A: Physical Geography*, *84*(1), 11–24. https://doi.org/10.1111/j.0435-3676.2002.00158.x

Halberstadt, A. R. W., Kowalewski, D. E., & DeConto, R. M. (2022). Reconciling persistent sub-zero temperatures in the McMurdo Dry Valleys, Antarctica, with Neogene dynamic marine ice-sheet fluctuations. *Geology*, *50*(5), 557–561. https://doi.org/10.1130/G49664.1

Hidy, A. J., Gosse, J. C., Pederson, J. L., Mattern, J. P., & Finkel, R. C. (2010). A geologically constrained Monte Carlo approach to modeling exposure ages from profiles of cosmogenic nuclides: An example from Lees Ferry, Arizona. *Geochemistry, Geophysics, Geosystems*, *11*(9). https://doi.org/10.1029/2010GC003084

Hidy, A. J., Gosse, J. C., Sanborn, P., & Froese, D. G. (2018). Age-erosion constraints on an Early Pleistocene paleosol in Yukon, Canada, with profiles of ^{10}Be and ^{26}Al: Evidence for a significant loess cover effect on cosmogenic nuclide production rates. *Catena*, *165*, 260–271. https://doi.org/10.1016/j.catena.2018.02.009

Ivy-Ochs, S., Schluchter, C., Kubik, P. W., Dittrich-Hannen, B., & Beer, J. (1995). Minimum ^{10}Be exposure ages of early Pliocene for the Table Mountain plateau and the sirius group at mount fleming, dry valleys, Antarctica. *Geology*, *23*(11), 1007–1010. https://doi.org/10.1130/0091-7613(1995)023<1007:MBEAOE>2.3.CO;2

Ivy-Ochs, S., Schlüchter, C., Prentice, M., Kubik, P. W., & Beer, J. (1997). ^{10}Be and ^{26}Al exposure ages for the sirius group at mount fleming, mount feather and Table Mountain and the plateau surface at Table Mountain. *The Antarctic Region: Geological Evolution and Processes, Terra Antarctica, Sienna*, 1153–1158.

Korschinek, G., Bergmaier, A., Faestermann, T., Gerstmann, U. C., Knie, K., Rugel, G., et al. (2010). A new value for the half-life of ^{10}Be by heavy-ion elastic recoil detection and liquid scintillation counting. *Nuclear Instruments and Methods in Physics Research Section B: Beam Interactions with Materials and Atoms*, *268*(2), 187–191. https://doi.org/10.1016/j.nimb.2009.09.020

Lal, D. (1991). Cosmic ray labeling of erosion surfaces: In situ nuclide production rates and erosion models. *Earth and Planetary Science Letters*, *104*(2), 424–439. https://doi.org/10.1016/0012-821X(91)90220-C

Lapalme, C. M., Lacelle, D., Pollard, W., Fortier, D., Davila, A., & McKay, C. P. (2017). Cryostratigraphy and the sublimation unconformity in permafrost from an ultraxerous environment, University Valley, McMurdo dry valleys of Antarctica. *Permafrost and Periglacial Processes*, *28*(4), 649–662. https://doi.org/10.1002/ppp.1948

Levy, R., Cody, R., Crampton, J., Fielding, C., Golledge, N., Harwood, D., et al. (2012). Reprint of: Late Neogene climate and glacial history of the Southern Victoria Land coast from integrated drill core, seismic and outcrop data. *Global and Planetary Change*, *96*(97), 157–180. https://doi.org/10.1016/j.gloplacha.2012.02.005

Lewis, A. R., Marchant, D. R., Ashworth, A. C., Hemming, S. R., & Machlus, M. L. (2007). Major middle Miocene global climate change: Evidence from east Antarctica and the transantarctic Mountains. *Bulletin of the Geological Society of America*, *119*(11–12), 1449–1461. https://doi.org/10.1130/0016-7606(2007)119[1449:MMMGCC]2.0.CO;2

Lifton, N., Sato, T., & Dunai, T. J. (2014). Scaling in situ cosmogenic nuclide production rates using analytical approximations to atmospheric cosmic-ray fluxes. *Earth and Planetary Science Letters*, *386*, 149–160. https://doi.org/10.1016/j.epsl.2013.10.052

Marchant, D. R., & Denton, G. H. (1996). Miocene and Pliocene paleoclimate of the dry valleys region, southern victoria land: A geomorphological approach. *Marine Micropaleontology*, *27*(1–4), 253–271. https://doi.org/10.1016/0377-8398(95)00065-8

Marchant, D. R., & Head, J. W. (2007). Antarctic dry valleys: Microclimate zonation, variable geomorphic processes, and implications for assessing climate change on Mars. *Icarus*, *192*(1), 187–222. https://doi.org/10.1016/j.icarus.2007.06.018

Marchant, D. R., Swisher, C. C., Lux, D. R., West, D. P., & Denton, G. H. (1993). Pliocene paleoclimate and East Antarctic ice-sheet history from surficial ash deposits. *Science*, *260*(5108), 667–670. https://doi.org/10.1126/science.260.5108.667

Marrero, S. M., Hein, A. S., Naylor, M., Attal, M., Shanks, R., Winter, K., et al. (2018). Controls on subaerial erosion rates in Antarctica. *Earth and Planetary Science Letters*, *501*, 56–66. https://doi.org/10.1016/j.epsl.2018.08.018

McKay, C. P., Mellon, M. T., & Friedmann, E. I. (1998). Soil temperatures and stability of ice-cemented ground in the McMurdo Dry Valleys, Antarctica. *Antarctic Science*, *10*(1), 31–38. https://doi.org/10.1017/s0954102098000054

Mifsud, C., Fujioka, T., & Fink, D. (2013). Extraction and purification of quartz in rock using hot phosphoric acid for in situ cosmogenic exposure dating. *Nuclear Instruments and Methods in Physics Research Section B: Beam Interactions with Materials and Atoms*, *294*, 203–207. https://doi.org/10.1016/j.nimb.2012.08.037

Morgan, D., Putkonen, J., Balco, G., & Stone, J. (2010). Quantifying regolith erosion rates with cosmogenic nuclides ^{10}Be and ^{26}Al in the McMurdo Dry Valleys, Antarctica. *Journal of Geophysical Research*, *115*(3), 1–17. https://doi.org/10.1029/2009JF001443

Morgan, D. J., Putkonen, J., Balco, G., & Stone, J. (2011). Degradation of glacial deposits quantified with cosmogenic nuclides, Quartermain Mountains, Antarctica. *Earth Surface Processes and Landforms*, *36*(2), 217–228. https://doi.org/10.1002/esp.2039

Naish, T., Powell, R., Levy, R., Wilson, G., Scherer, R., Talarico, F., et al. (2009). Obliquity-paced Pliocene west Antarctic ice sheet oscillations. *Nature*, *458*(7236), 322–328. https://doi.org/10.1038/nature07867

Ng, F., Hallet, B., Sletten, R. S., & Stone, J. O. (2005). Fast-growing till over ancient ice in Beacon valley, Antarctica. *Geology*, *33*(2), 121–124. https://doi.org/10.1130/G21064.1

Nishiizumi, K. (2004). Preparation of ^{26}Al AMS standards. *Nuclear Instruments and Methods in Physics Research Section B: Beam Interactions with Materials and Atoms*, *223–224*, 388–392. https://doi.org/10.1016/j.nimb.2004.04.075

Nishiizumi, K., Imamura, M., Caffee, M. W., Southon, J. R., Finkel, R. C., & McAninch, J. (2007). Absolute calibration of ^{10}Be AMS standards. *Nuclear Instruments and Methods in Physics Research Section B: Beam Interactions with Materials and Atoms*, *258*(2), 403–413. https://doi.org/10.1016/j.nimb.2007.01.297

Patterson, M. O., McKay, R., Naish, T., Escutia, C., Jimenez-Espejo, F. J., Raymo, M. E., et al. (2014). Orbital forcing of the East Antarctic ice sheet during the Pliocene and early Pleistocene. *Nature Geoscience*, *7*(11), 841–847. https://doi.org/10.1038/ngeo2273

Pringle, D. J., Dickinson, W. W., Trodahl, H. J., & Pyne, A. R. (2003). Depth and seasonal variations in the thermal properties of Antarctic Dry Valley permafrost from temperature time series analysis. *Journal of Geophysical Research*, *108*(B10), 1–13. https://doi.org/10.1029/2002jb002364

Putkonen, J., Balco, G., & Morgan, D. (2008). Slow regolith degradation without creep determined by cosmogenic nuclide measurements in Arena Valley, Antarctica. *Quaternary Research*, *69*(2), 242–249. https://doi.org/10.1016/j.yqres.2007.12.004

Salvatore, M. R., & Levy, J. S. (2021). *Chapter 11: The McMurdo dry Valleys of Antarctica: A geological environment and ecological analog to the Martian surface and near surface* (pp. 291–332). Mars Geological Enigmas. Elsevier Inc. https://doi.org/10.1016/B978-0-12-820245-6/00011-2

Shakun, J. D., Corbett, L. B., Bierman, P. R., Underwood, K., Rizzo, D. M., Zimmerman, S. R., et al. (2018). Minimal East Antarctic Ice Sheet retreat onto land during the past eight million years. *Nature*, *558*, 284–287. https://doi.org/10.1038/s41586-018-0155-6

Sheldrick, B. H. (1984). Analytical methods manual. *Water Quality Bulletin*(84), 4.

Sugden, D. E., Marchant, D. R., & Denton, G. H. (1993). The case for a stable East Antarctic ice sheet: The background. *Geografiska Annaler. Series A, Physical Geography, A Special VolumeArising from the Vega Symposium: The Case for a Stable East Antarctic Ice Sheet*, *75*(4), 151–154. https://doi.org/10.1080/04353676.1993.11880392

Sugden, D. E., Marchant, D. R., Potter, N., Souchez, R. A., Denton, G. H., Swisher, C. C., & Tison, J. L. (1995). Preservation of Miocene glacier ice in east Antarctica. *Nature*, *376*(6539), 412–414. https://doi.org/10.1038/376412a0

Valletta, R. D., Willenbring, J. K., Lewis, A. R., Ashworth, A. C., & Caffee, M. (2015). Extreme decay of meteoric beryllium-10 as a proxy for persistent aridity. *Scientific Reports*, *5*, 1–7. https://doi.org/10.1038/srep17813

Verret, M., Trinh-Le, C., Dickinson, W., Norton, K., Lacelle, D., Christl, M., et al. (2023). Late Miocene onset of hyper-aridity in East Antarctica indicated by meteoric beryllium-10 in permafrost. *Nature Geoscience*, *16*(6), 492–498. https://doi.org/10.1038/s41561-023-01193-4

Wilcken, K. M., Fujioka, T., Fink, D., Fülöp, R. H., Codilean, A. T., Simon, K., et al. (2019). SIRIUS performance: ^{10}Be, ^{26}Al and ^{36}Cl measurements at ANSTO. *Nuclear Instruments and Methods in Physics Research, Section B: Beam Interactions with Materials and Atoms*, *455*, 300–304. https://doi.org/10.1016/j.nimb.2019.02.009

21699011, 2025, 3, Downloaded from https://agupubs.onlinelibrary.wiley.com/doi/10.1029/2024JF007911 by University Of Burgos, Wiley Online Library on [12/03/2026]. See the Terms and Conditions (https://onlinelibrary.wiley.com/terms-and-conditions) on Wiley Online Library for rules of use; OA articles are governed by the applicable Creative Commons License